A PRC2-Kdm5b axis sustains tumorigenicity of acute myeloid leukemia

Zhihong Ren[a,b,1,2], Arum Kim[a,b,1], Yu-Ting Huang[c,3], Wen-Chieh Pi[c,3], Weida Gong[a], Xufen Yu[d], Jun Qi[e], Jian Jin[d], Ling Cai[a,b,f], Robert G. Roeder[g,4], Wei-Yi Chen[c,h,4], and Gang Greg Wang[a,b,i,4]

[a]Lineberger Comprehensive Cancer Center, University of North Carolina at Chapel Hill School of Medicine, Chapel Hill, NC 27599; [b]Department of Biochemistry and Biophysics, University of North Carolina at Chapel Hill School of Medicine, Chapel Hill, NC 27599; [c]Institute of Biochemistry and Molecular Biology, National Yang Ming Chiao Tung University, Taipei 112, Taiwan; [d]Mount Sinai Center for Therapeutics Discovery, Departments of Pharmacological Sciences and Oncological Sciences, Tisch Cancer Institute, Icahn School of Medicine at Mount Sinai, New York, NY 10029; [e]Department of Cancer Biology, Dana-Farber Cancer Institute, Boston, MA 02215; [f]Department of Genetics, University of North Carolina at Chapel Hill School of Medicine, Chapel Hill, NC 27599; [g]Laboratory of Biochemistry and Molecular Biology, The Rockefeller University, New York, NY 10065; [h]Cancer Progression Research Center, National Yang Ming Chiao Tung University, Taipei 112, Taiwan; and [i]Department of Pharmacology, University of North Carolina at Chapel Hill School of Medicine, Chapel Hill, NC 27599

Contributed by Robert G. Roeder; received December 19, 2021; accepted January 20, 2022; reviewed by Hao Jiang and Zhijian Qian

Acute myeloid leukemias (AMLs) with the NUP98-NSD1 or mixed lineage leukemia (MLL) rearrangement (MLL-r) share transcriptomic profiles associated with stemness-related gene signatures and display poor prognosis. The molecular underpinnings of AML aggressiveness and stemness remain far from clear. Studies with EZH2 enzymatic inhibitors show that polycomb repressive complex 2 (PRC2) is crucial for tumorigenicity in NUP98-NSD1$^+$ AML, whereas transcriptomic analysis reveal that *Kdm5b*, a lysine demethylase gene carrying "bivalent" chromatin domains, is directly repressed by PRC2. While ectopic expression of Kdm5b suppressed AML growth, its depletion not only promoted tumorigenicity but also attenuated anti-AML effects of PRC2 inhibitors, demonstrating a PRC2–|*Kdm5b* axis for AML oncogenesis. Integrated RNA sequencing (RNA-seq), chromatin immunoprecipitation followed by sequencing (ChIP-seq), and Cleavage Under Targets & Release Using Nuclease (CUT&RUN) profiling also showed that Kdm5b directly binds and represses AML stemness genes. The anti-AML effect of Kdm5b relies on its chromatin association and/or scaffold functions rather than its demethylase activity. Collectively, this study describes a molecular axis that involves histone modifiers (PRC2–|*Kdm5b*) for sustaining AML oncogenesis.

PRC2 | Kdm5b | stemness | tumorigenicity | AML

Acute myeloid leukemia (AML) is a common form of childhood cancer (affecting patients age 0 to 15 y), and despite improvement, its prognosis remains generally poor. In particular, chromosomal abnormality of NUP98-NSD1 (1–3) and MLL rearrangements (MLL-r) (4, 5) account, respectively, for ~5 to 16% and 15 to 20% of pediatric AML cases. Acute lymphoblastic leukemia with MLL-r is more prevalent in pediatric patients. These patients with NUP98-NSD1 or MLL-r generally show particularly poor outcomes in the clinic, demanding more effective therapeutics. There is a need to better understand the molecular underpinnings of tumorigenesis and aggressiveness in these AMLs. The translocation of NUP98-NSD1 generates a chimeric protein that fuses the N-terminal segment of NUP98, enriched in the intrinsically disorganized region causing liquid–liquid phase separation (6), with a C-terminal region of NSD1, which contains histone-methyltransferase and chromatin-binding domains (1–3, 7), whereas MLL-r chimeras fuse an N-terminal MLL segment that interacts with Menin and LEDGF with a C-terminal part of an MLL-r fusion partner such as AF9, ENL, or AF4 (4, 5, 8). Previous studies using murine and human AMLs have collectively shown that both NUP98-NSD1 and MLL-r oncoproteins (such as MLL-AF9 and MLL-AF4) directly bind and activate a set of stemness- and proliferation-related gene targets, notably the Hox cluster genes, thereby potentiating AML tumorigenesis (1–3, 5, 7, 8). It remains to be fully understood how these AMLs sustain tumorigenicity.

Chromatin modulation is increasingly appreciated to be pivotal for malignant development (9–12). Previously, it has been shown that MLL-r$^+$ AMLs rely partly on polycomb repressive complex 2 (PRC2) for maintaining tumorigenesis, implicative of an attractive therapeutic target (13–17). However, it remains far from clear which molecular pathways are responsible for oncogenic actions of PRC2 in AML. In this study, we show that NUP98-NSD1$^+$ AML cells are exquisitely sensitive to an inhibitor of PRC2 enzymatic activity, thus extending PRC2 dependency to multiple subtypes of genetically defined AMLs displaying poor prognosis. Our transcriptomic profiling in AML further identified Kdm5b (also known as Jarid1b, Plu-1, or RBP2-H1), a multifunctional demethylase that can remove histone H3 lysine 4 tri/di-methylation (H3K4me3/2), to be a

Significance

Acute myeloid leukemias (AMLs) with NUP98-NSD1 or MLL abnormality are generally aggressive, demanding a better understanding of the underlying oncogenic mechanisms. We show that these AMLs rely on a regulatory axis involving PRC2–|*Kdm5b*–|stemness genes for sustaining an oncogenic program. The H3K27 methylase activity of polycomb repressive complex 2 (PRC2) is crucial for repressing Kdm5b, a corepressor carrying a H3K4me3 reader domain, that antagonizes the AML oncoproteins by directly binding to and down-regulating the AML stemness genes, thereby suppressing acute leukemogenesis. Such an AML-suppressing role of Kdm5b is not dependent on its intrinsic demethylase activity but requires its scaffold and/or chromatin association functions. The findings of this study shall aid in potential therapeutics of the affected AML patients.

Author contributions: Z.R. and G.G.W. designed research; Z.R., A.K., Y.-T.H., W.-C.P., W.G., X.Y., J.Q., J.J., and L.C. performed research; R.G.R. and W.-Y.C. contributed new reagents/analytic tools; A.K., Y.-T.H., W.-C.P., W.G., X.Y., J.Q., J.J., L.C., R.G.R., W.-Y.C., and G.G.W. analyzed data; and Z.R., A.K., R.G.R., W.-Y.C., and G.G.W. wrote the paper.

Reviewers: H.J., University of Virginia; and Z.Q., University of Florida.

The authors declare no competing interest.

See online for related content such as Commentaries.

[1]Z.R. and A.K. contributed equally to this work.

[2]Present address: Division of Hematologic Malignancies, Johns Hopkins University School of Medicine, Baltimore, MD 21287.

[3]Y.-T.H. and W.-C.P. contributed equally to this work.

[4]To whom correspondence may be addressed. Email: roeder@rockefeller.edu, chenwy@nycu.edu.tw, or greg_wang@med.unc.edu.

This article contains supporting information online at http://www.pnas.org/lookup/suppl/doi:10.1073/pnas.2122940119/-/DCSupplemental.

Published February 25, 2022.

CELL BIOLOGY

critical downstream target repressed by PRC2. Depletion of Kdm5b not only promoted AML development but also significantly desensitized AML cells to the PRC2 inhibitor, thus uncovering an involvement of the PRC2–|*Kdm5b* axis for AML tumorigenesis. Genomic profiling by chromatin immunoprecipitation followed by sequencing (ChIP-seq), Cleavage Under Targets & Release Using Nuclease (CUT&RUN), and RNA-seq further showed that both Kdm5b and NUP98-NSD1 are targeted to stemness- and proliferation-related genes and that Kdm5b functions to suppress a suite of AML proto-oncogenes. Systematic mutagenesis showed Kdm5b's intrinsic demethylase activity to be dispensable for AML suppression, whereas its chromatin-binding functions are essential, indicating a scaffolding role of Kdm5b in assembling the chromatin-bound complex for transcriptional repression. Together, this study unveils a PRC2–|*Kdm5b*–|stemness axis that operates to promote AML oncogenesis and aggressiveness, which sheds light on potential therapeutic means.

Results

NUP98-NSD1$^+$ AML Cells Are Sensitive to Enzymatic Inhibitor of PRC2. Previously, it has been shown that UNC1999, a selective inhibitor of the PRC2 catalytic subunit (EZH2 or EZH1), suppressed growth of MLL-r AML cells (17). Here, we treated murine AML cells established by NUP98-NSD1 (7) with UNC1999. Following the depletion of global H3K27me3 (Fig. 1*A*, *Inset*), we observed a robust response and sensitivity to UNC1999, comparable to what was seen with MLL-r AML (17). Relative to mock treatment, UNC1999 dramatically suppressed the in vitro proliferation (Fig. 1*A*) and colony formation of NUP98-NSD1$^+$ AML cells (Fig. 1*B*). Treatment with UNC1999 also resulted in enhanced cell differentiation (Fig. 1*C*), increased apoptosis (Fig. 1*D* and *SI Appendix*, Fig. S1), and slower cell cycle progression (Fig. 1*E*) in AML cells. Furthermore, when compared to vehicle treatment, UNC1999 treatment also significantly delayed tumor progression in the murine NUP98-NSD1$^+$ AML model (Fig. 1*F*). Taken together, these results demonstrate a PRC2 dependency for the NUP98-NSD1–associated AML growth.

Transcriptomic Profiling Identified *Kdm5b* to Be a PRC2-Repressed Gene in AML with NUP98-NSD1 or MLL-r. In order to dissect downstream mediators through which PRC2 sustains AML oncogenesis, we conducted transcriptomic profiling of NUP98-NSD1$^+$ AML cells posttreatment with PRC2 inhibitors. To rule out a potential off-target effect, we treated NUP98-NSD1$^+$ AML cells either with UNC1999 or with a second PRC2 inhibitor, JQEZ5 (18, 19), and then performed RNA-seq analysis (Dataset S1 and *SI Appendix*, Fig. S2*A*). Replicated RNA-seq profiles within the same treatment group were highly consistent (*SI Appendix*, Fig. S2*B*), and transcripts showing the increased expression after treatment with either of the two inhibitors also overlapped significantly (Fig. 2*A* and *SI Appendix*, Fig. S2*C*), although the overall effect of JQEZ5 was somewhat milder (please note a milder overall change in gene expression caused by JQEZ5, compared to UNC1999, as revealed by principal component analysis, PC1 of *SI Appendix*, Fig. S2*B*). Gene set enrichment analysis (GSEA) showed the blockade of PRC2's enzymatic activity by either inhibitor to be correlated with up-regulation of transcripts repressed by PRC2 or those related either to leukocyte differentiation or apoptosis (Fig. 2*B* and *SI Appendix*, Fig. S2 *D* and *E*), consistent with the observed cell phenotypes posttreatment (Fig. 1). To further identify genes commonly repressed by PRC2 in NUP98-NSD1$^+$ and MLL-r AMLs, we compared UNC1999-derepressed transcripts identified in the two AMLs and, to further enhance the rigor, also included our previous transcriptomic data for knockdown of the essential component of PRC2, Eed (17) (Fig. 2*C*). This analysis identified a 31-gene signature that is commonly up-regulated among all three comparisons (Fig. 2*C* and *SI Appendix*, Table S1) and included *Cdkn2a*, a cell cycle inhibitor gene known to be directly repressed by PRC2 (17). In addition, *Kdm5b*, encoding a histone demethylase shown to have a tumor-suppressive role in MLL-r AML (20), was also found to be significantly activated upon PRC2 inhibition (Fig. 2*C*). The qRT-PCR assays verified the marked up-regulation of *Kdm5b* following either PRC2 enzymatic inhibition (Fig. 2*D*) or EZH2 depletion (*SI Appendix*, Fig. S2*F*) in independent AML cell lines.

To assess whether *Kdm5b* is a direct target of PRC2 and H3K27me3, we examined H3K27me3 and H3K4me3 ChIP-seq data that we previously generated in MLL-AF9–transformed murine AML cells (17) and found the *Kdm5b* promoter to be demarcated with both histone marks (Fig. 2*E*), which is a characteristic of bivalent domains in chromatin. We also conducted ChIP-seq in MV4;11 cells, a human AML line harboring MLL-AF4, and also found *KDM5B* to be directly bound by EZH2 and H3K4me3 (Fig. 2*E*). Interrogation of multiple clinical outcome datasets of human AML patients, including the TCGA AML cohort, consistently displayed a positive correlation between the lower *KDM5B* expression and the significantly poorer prognosis (Fig. 2*F*). Collectively, these observations support the view that *KDM5B* is dynamically regulated, with PRC2-catalyzed H3K27me3 serving as a critical repressor, and that *KDM5B* expression is a predictive marker of AML prognosis.

Kdm5b Depletion not only Promotes AML Oncogenesis but also Significantly Desensitizes AML Cell Response to PRC2 Inhibition. Kdm5b depletion in the NUP98-NSD1$^+$ AML cells resulted in the significantly accelerated proliferation (*SI Appendix*, Fig. S3*A*) and increased colony formation in the in vitro assays (Fig. 3 *A* and *B*; see DMSO, *Right* versus *Left*). Compared to mock treatment, Kdm5b depletion also significantly accelerated AML development in syngeneic mice (Fig. 3*C*; see black lines, dashed versus solid), consistent with what was previously observed with MLL-r AML (20). Importantly, Kdm5b depletion significantly attenuated the AML cell sensitivity to UNC1999 in both liquid cultures (*SI Appendix*, Fig. S2*B*) and colony formation assays (Fig. 3*A*). Relative to mock treatment, Kdm5b depletion completely abrogated the UNC1999-mediated suppression of AML growth in mice (Fig. 3*C*; see dashed lines, black versus red). These results demonstrated a tumor-suppressive role for Kdm5b and an oncogenic axis involving PRC2–|*Kdm5b* in NUP98-NSD1$^+$ AMLs.

RNA-seq Profiling Shows a Role of Kdm5b in Suppressing a Stemness-Related Gene-Expression Program in AML. To examine the gene-regulatory role for Kdm5b in NUP98-NSD1$^+$ AMLs, we carried out RNA-seq profiling after Kdm5b depletion, which revealed transcripts showing the altered expression due to Kdm5b loss (Fig. 3*D* and Dataset S2). GSEA using RNA-seq profiles revealed a negative correlation between Kdm5b depletion and the differentiation-related gene sets (Fig. 3*E*). Furthermore, GSEA of RNA-seq profiles obtained after ectopic Kdm5b expression in MLL-AF9$^+$ AML cells (Dataset S3) revealed a positive correlation between Kdm5b expression and gene sets related to differentiation, apoptosis, or slowed cell proliferation (Fig. 3*F* and *SI Appendix*, Fig. S3 *D* and *E*). Despite the cell background difference, there is a significant overlap between the Kdm5b-repressed transcripts in the two AML models, including genes, such as Sox4, Id2, Myb, Brd3, Hmga2, and Hmgb3, known to be essential for AML stemness or differentiation arrest (Fig. 3*G* and *SI Appendix*, Table S2). Interestingly, oncogenes such as Kras and cell cycle–related genes that include Ccnd1, Ccnd2, and Ccne2 were also found to be repressed by Kdm5b (Fig. 3*G*). These results thus link Kdm5b to AML-related gene-expression programs.

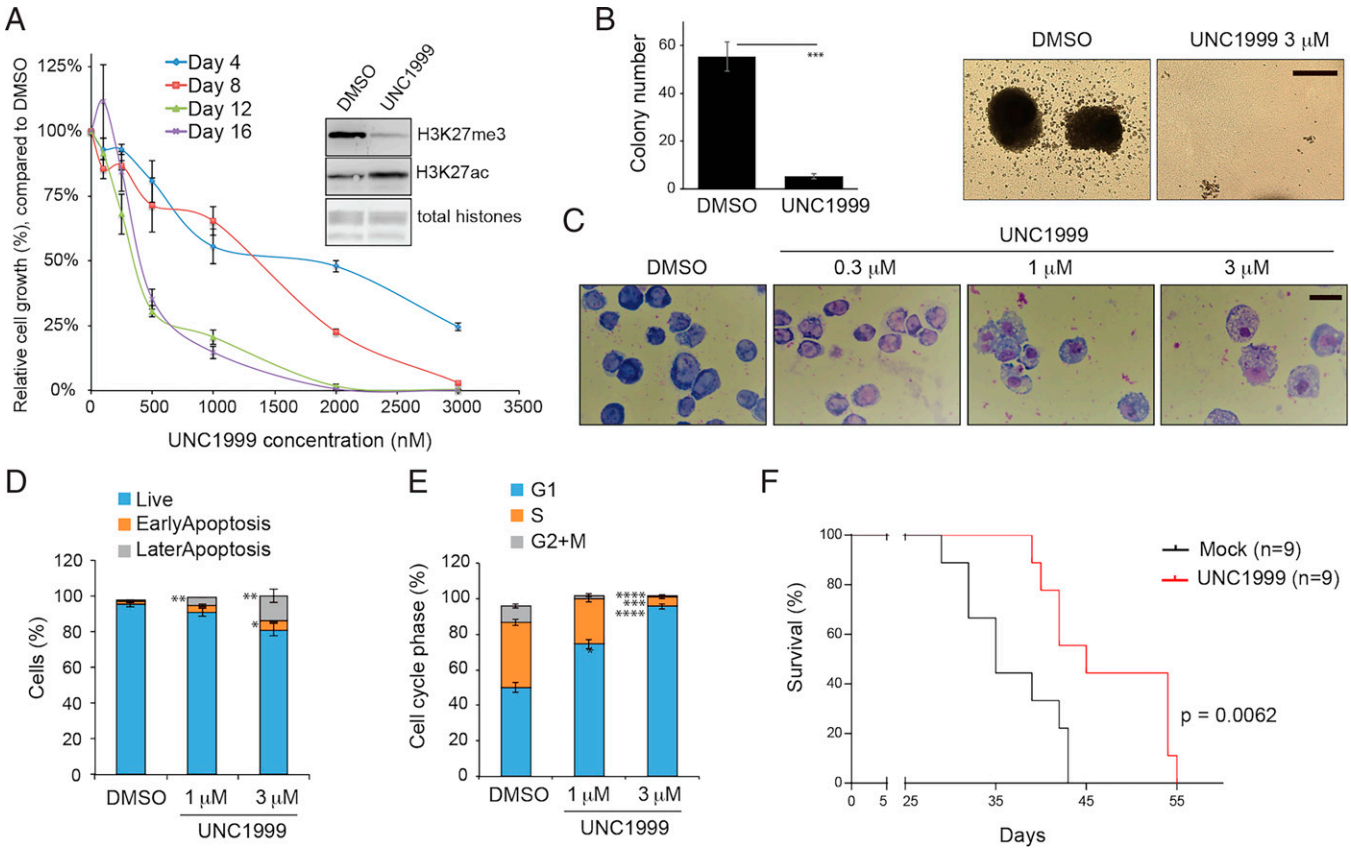

Fig. 1. PRC2 sustains tumorigenesis in the NUP98-NSD1$^+$ AML. (*A*) Proliferation of NUP98-NSD1–transformed murine AML cells after treatment with UNC1999, an enzymatic inhibitor of EZH2/1, for the indicated duration. The *y*-axis represents the relative percentage of cell numbers in cultures, normalized to dimethyl sulfoxide (DMSO) treatment ($n = 3$ independent experiments; shown as mean ± SD). *Inset* shows immunoblotting of global H3K27me3 and H3K27ac after a 24-h treatment with 3 μM of UNC1999, relative to DMSO. (*B*) Quantification of CFUs (*Left*) and images of representative single-cell colonies (*Right*) formed by NUP98-NSD1$^+$ AML cells, cultured in the semisolid medium containing DMSO or 3 μM of UNC1999 for 10 d ($n = 3$ independent experiments; mean ± SD; unpaired two-tailed Student's *t* test). ***$P < 0.001$. (Scale bar, 2 mm.) (*C*) Wright–Giemsa staining images showing the differentiation status of NUP98-NSD1$^+$ AML cells, treated with DMSO or the indicated concentration of UNC1999 for 4 d. (Black bar, 10 μm.) (*D* and *E*) Summary of apoptotic cells, analyzed by propidium iodide (PI), and annexin-V staining (*D*), and cell cycle progress, analyzed by PI-based DNA staining (*E*), in the NUP98-NSD1$^+$ AML cells, following a 2-d treatment with DMSO or the indicated concentration of UNC1999 ($n = 3$ independent experiments; mean ± SD; unpaired two-tailed Student's *t* test). *$P < 0.05$; **$P < 0.01$; ***$P < 0.001$; ****$P < 0.0001$. (*F*) Kaplan–Meier curve showing kinetics of NUP98-NSD1-induced AML in a transplantation model using syngeneic mice. Starting from day 7 posttransplantation, mice received oral administration of either vehicle (blue) or 100 mg/kg UNC1999 (red) once per day. n, cohort size. Statistical significance was determined by log-rank test.

ChIP-seq Data Establish Direct Cobinding of Kdm5b and NUP98-NSD1 to AML-Related Target Genes, Thus Providing a Molecular Explanation for Antagonism between KDM5B and AML Oncoproteins. To further address whether Kdm5b directly regulates the AML-related gene program, we conducted ChIP-seq for Kdm5b, NUP98-NSD1 (flag-tagged), and H3K4me3 in NUP98-NSD1$^+$ AML cells (Datasets S4 and S5). Notably, our results revealed a significant coexistence of the three factors at gene promoters (Fig. 4 *A* and *B*), which is in good agreement with previous reports that the C-terminal PHD finger domain of Kdm5b directly binds H3K4me3 (21, 22) and that Kdm5b binding sites overlap H3K4me3 in different cell models (23, 24); also, chimeric NUP98 fusion oncoproteins (NUP98-NSD1 or NUP98-PHD) were found targeted to promoters for oncogene activation (7, 25–27). Integrated analyses of our ChIP-seq and RNA-seq datasets in NUP98-NSD1$^+$ AML cells further defined genes that are cotargeted by both Kdm5b and NUP98-NSD1 and also transcriptionally repressed by Kdm5b (Fig. 4*B* and *SI Appendix*, Table S3), which again included a suite of AML proliferative and stemness genes such as Brd3, Ccnd3, Kras, Sox4, and Hoxa7 (Fig. 4 *C*–*F* and *SI Appendix*, Fig. S4). These results demonstrate a direct suppressing effect by Kdm5b on the oncogenic gene-expression program, thereby antagonizing AML-promoting effects by oncoproteins.

Kdm5b's Chromatin Association Domains Are Essential for Its AML Suppressive Role, whereas Its Demethylase Activity Is Dispensable. Kdm5b is a large protein with multiple functional motifs. Besides a Jumonji (Jmj) domain, essential for lysine demethylation, Kdm5b contains three PHD fingers, with the first and third ones specifically binding nonmodified (H3K4me0) and highly methylated (e.g., H3K4me3) H3K4, respectively, as well as an ARID domain previously shown to bind CG-rich DNA (28) (Fig. 5*A*). To examine potential involvement of these functional domains in Kdm5b-mediated AML suppression, we ectopically expressed Kdm5b in the NUP98-NSD1$^+$ AML cells. Here, we employed a set of Kdm5b mutants exhibiting the abolished activity in either chromatin binding or demethylation (Fig. 5*A*). These mutants included K164E/S168D (in the Arid domain) (28), D328A (in PHD1) (21, 22), H499A (demethylase dead) (29, 30), ΔPHD2 (PHD2 deletion), and W1501A (in PHD3) (22, 26). Wild-type (WT) and mutant forms of Kdm5b showed comparable levels of expression (Fig. 5*B*). Compared to mock, WT Kdm5b robustly suppressed AML growth in vitro (Fig. 5*C*; see WT) and in mice, as assessed by assessment of the in vivo expansion of luciferase/GFP-labeled AML cells via live animal imaging and fluorescence-activated cell sorting (FACS) with the isolated cells from killed mice (Fig. 5 *D* and *E*; see

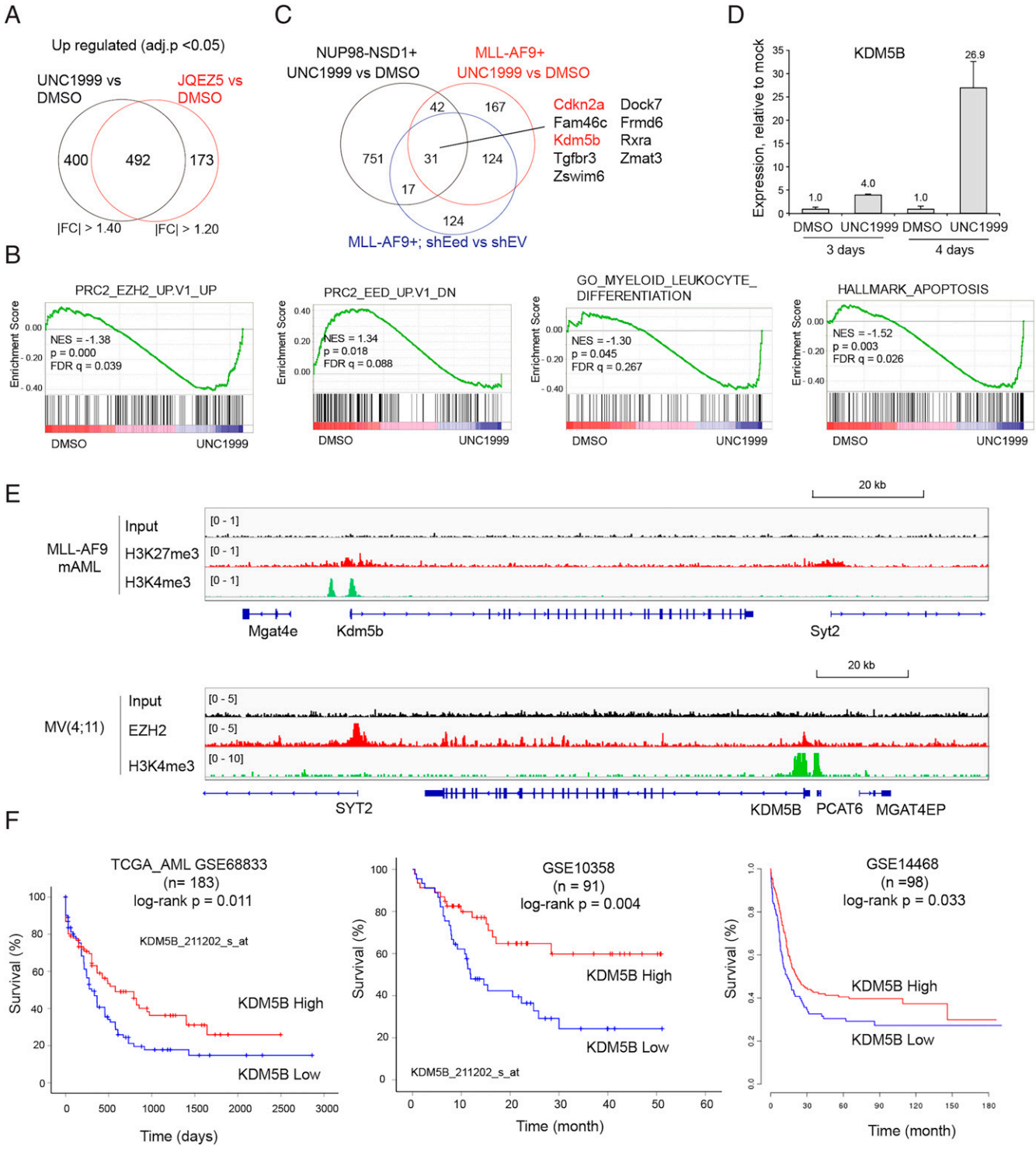

Fig. 2. *Kdm5b*, encoding a tumor suppressor of AML, is a direct target of PRC2 and H3K27me3 in AML. (*A*) Venn diagram showing the overlap between DEGs, as determined by RNA-seq to be up-regulated in NUP98-NSD1$^+$ AML cells after a 4-d treatment with 3 μM of independent PRC2 inhibitors, either UNC1999 (*Left*) or JQEZ5 (*Right*), relative to DMSO (n = 3 replicated samples). Threshold of DEG is set as adjusted DESeq calculated probability value (adj.p) < 0.05, the indicated fold-change (FC) cutoff, and mean tag counts >10. (*B*) GSEA revealing that enzymatic inhibition of PRC2 by UNC1999 is positively correlated to activation of the indicated PRC2-repressed, myeloid differentiation–related, or apoptosis-related gene signature in the NUP98-NSD1$^+$ AML cells. NES, normalized enrichment score; FDR, false discovery rate. (*C*) Venn diagram showing overlap among the DEGs up-regulated posttreatment of NUP98-NSD1$^+$ (black) or MLL-AF9$^+$ AML cells (red) with UNC1999, or postknockdown of Eed, an essential PRC2 component, in the latter cells, relative to the respective controls. (*D*) qRT-PCR for *Kdm5b* in MLL-AF9$^+$ murine AML cells treated with 3 μM of UNC1999 for the indicated duration, relative to DMSO (n = 3 independent experiments; shown as mean ± SD). The y-axis represents PCR signals relative to DMSO-treated cells after normalization to GAPDH. (*E*) ChIP-seq profiles of H3K27me3 or EZH2 and H3K4me3 at the *Kdm5b* gene in MLL-AF9$^+$ murine AML (mAML) cells (*Upper*) and MV4;11 cells, an MLL-AF4$^+$ human AML line (*Lower*). (*F*) Kaplan–Meier survival curve for *KDM5B* expression in the indicated AML patients, including the TCGA cohort (*Left*). Statistical significance was determined by log-rank test. n, cohort size.

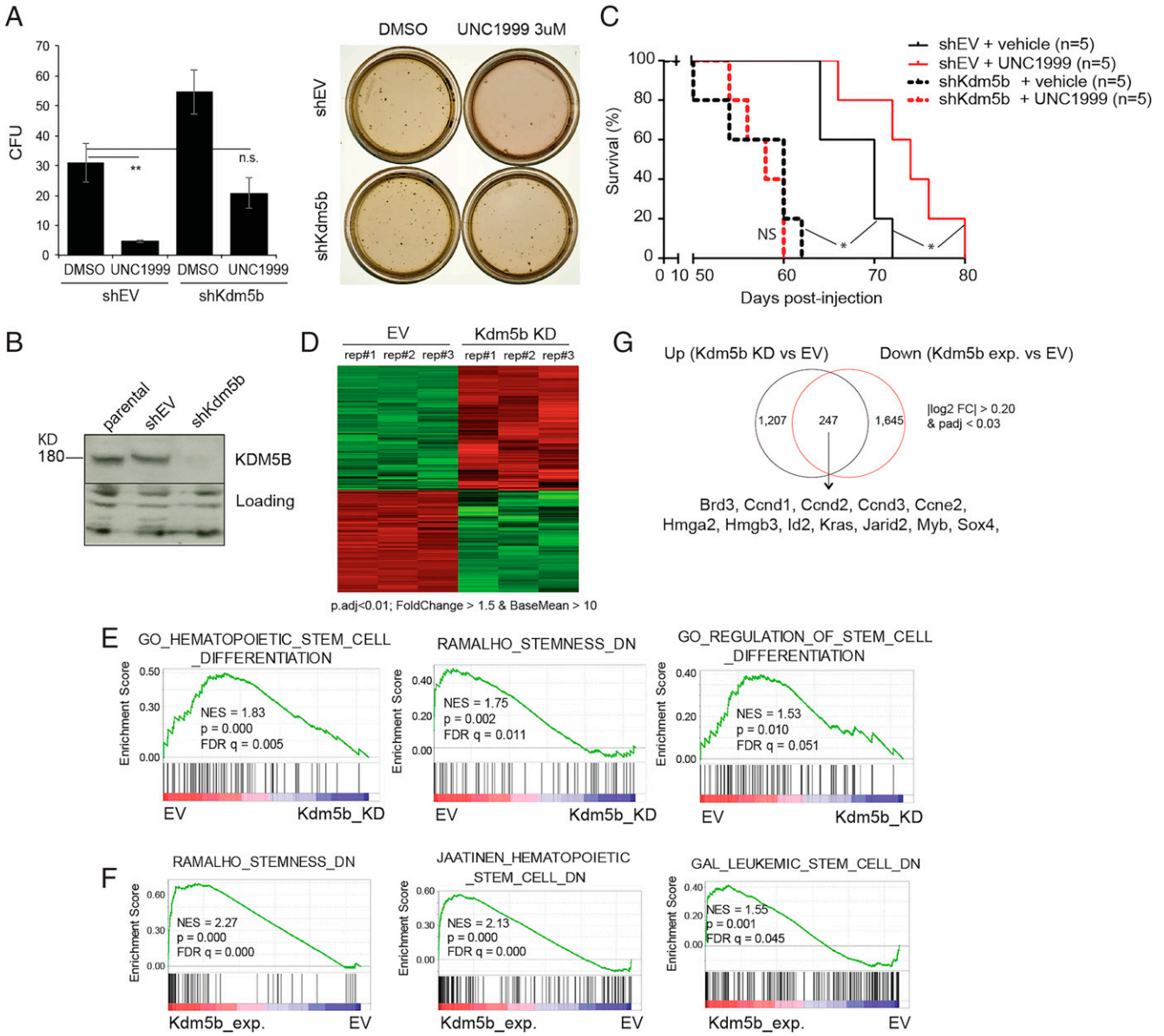

Fig. 3. Depletion of Kdm5b not only renders AML cells unresponsive to PRC2 inhibition but also promotes aggressiveness of AML. (*A*) Quantification of CFU (*Left*; $n = 3$ independent experiments; mean ± SD; unpaired two-tailed Student's *t* test) and image of single-cell colonies (*Right*) formed by NUP98-NSD1$^+$ murine AML cells, transduced with either EV (shEV) or Kdm5b-targeting shRNA (shKdm5b), after a 10-d cultivation in the semisolid medium containing either DMSO or 3 μM of UNC1999. $^{**}P < 0.01$; n.s., not significant. (*B*) Immunoblotting of Kdm5b after Kdm5b depletion. (*C*) Survival curve showing the kinetics of murine AMLs induced by NUP98-NSD1$^+$ cells, which were stably transduced with vector (shEV; solid lines) or Kdm5b-targeting shRNA (shKdm5b; dashed lines), in syngeneic mice ($n = 5$) treated with either vehicle (black) or UNC1999 (red). Statistical significance was determined by log-rank test. $^*P < 0.05$; NS, not significant. (*D*) Heatmap of RNA-seq results showing relative expression of DEGs in NUP98-NSD1$^+$ murine AML cells after Kdm5b knockdown (KD), relative to mock (EV). Threshold of DEG is indicated. $n = 3$ biological replicates (rep.). (*E*) GSEA shows a negative correlation between Kdm5b knockdown (Kdm5b_KD) and the indicated differentiation-related gene sets in NUP98-NSD1$^+$ murine AML cells ($n = 3$ replicated samples). (*F*) GSEA shows a positive correlation between ectopic expression of Kdm5b (Kdm5b_exp.) and the indicated differentiation-related gene sets in MLL-AF9$^+$ murine AML cells ($n = 2$ replicated samples). (*G*) Venn diagram showing overlap between the up-regulated transcripts after Kdm5b KD (*Left*) and the down-regulated transcripts after ectopic Kdm5b expression (Kdm5b exp.) (*Right*) relative to their respective controls, as determined by RNA-seq in AML cells. AML-related oncogenes and the DEG threshold are labeled. padj, adjusted *P* values.

WT). As a result, the typical splenomegaly seen with the NUP98-NSD1–induced murine AML was suppressed by WT Kdm5b compared to mock, and leukemogenesis was significantly delayed (Fig. 5 *F* and *G*; see WT versus empty vector [EV]). These results are in agreement with the positive correlation between the higher *KDM5B* expression and improved clinical outcomes of AML patients (Fig. 2*F*). In contrast, all of the tested chromatin-binding mutations, including K164E/S168D (ARID), D328A (PHD1), and W1501A (PHD3), almost completely abolished Kdm5b's anti-AML effects both in vitro (Fig 5 *B* and *C*) and in vivo (Fig. 5 *D*–*G*; see chromatin-binding mutants versus WT). Unexpectedly, the Kdm5b H499A mutant, which lacks the H3K4me3 demethylase activity (29, 30), retained the tumor-suppressive activity at a level comparable to what was observed for WT (Fig. 5 *C*–*G*; H499A versus WT). These observations in the NUP98-NSD1$^+$ AML model indicate essential

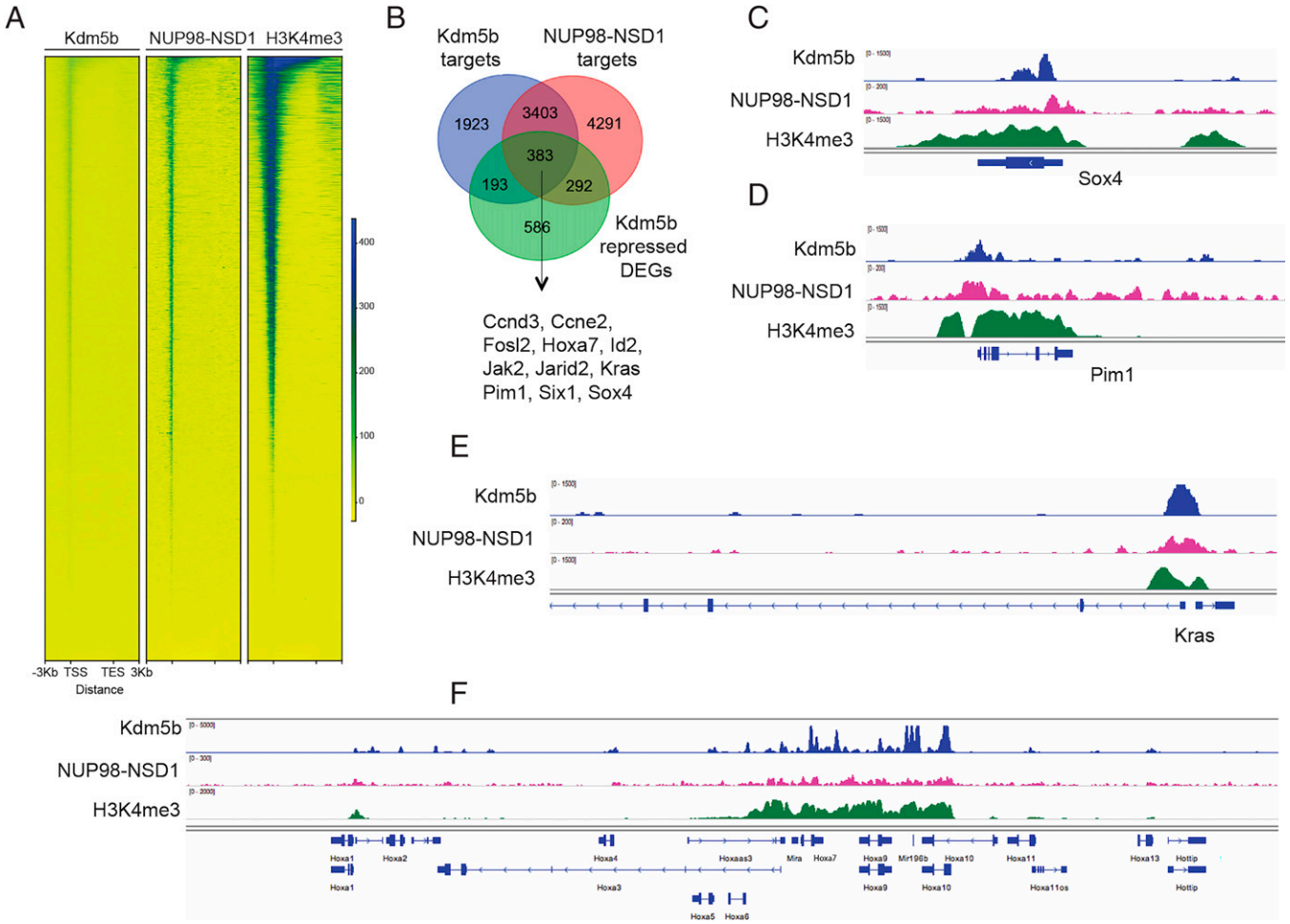

Fig. 4. Both Kdm5b and the leukemic oncoprotein, NUP98-NSD1, directly bind to stemness-related and AML-causing genes. (*A*) Heatmap showing ChIP-seq signals of Kdm5b, Flag-tagged NUP98-NSD1, and H3K4me3 at promoter-proximal regions (±3 kb from transcriptional start site [TSS] of all genes) in NUP98-NSD1$^+$ AML cells. TES, transcriptional end site. (*B*) Venn diagram showing the overlap among gene targets directly bound by Kdm5b (blue) or NUP98-NSD1 (red) and the Kdm5b-repressed genes (green; based on RNA-seq) in NUP98-NSD1$^+$ AML cells. (*C–F*) Integrative genomics viewer (IGV) views showing ChIP-seq profiles (input depth–normalized) of Kdm5b, NUP98-NSD1, and H3K4me3 at genes related to AML cell proliferation and stemness such as Sox4 (*C*), Pim1 (*D*), Kras (*E*), and Hox-a (*F*).

requirements for Kdm5b's chromatin association and/or scaffolding functions for suppressing leukemogenesis, whereas its intrinsic demethylase activity is dispensable.

To further assess the role of the Kdm5b demethylase activity during leukemogenesis, we employed MLL-AF9–transformed AML as a second model and confirmed comparable suppressive effects by WT Kdm5b and its H499A mutant on AML cell proliferation when compared to mock (Fig. 6 *A* and *B*). It has been reported that Kdm5b or related Kdm5a associates with the nucleosome remodeling and deacetylase (NuRD) complex, which has histone deacetylase (such as HDAC1) and gene-repressive activities (22, 31, 32). Coimmunoprecipitation (CoIP) showed that both WT and H499A-mutated Kdm5b associated with HDAC1 (Fig. 6*C*), a strong transcriptional corepressor. These results indicate a scaffolding role, rather than an intrinsic demethylase function, for Kdm5b in suppressing AML. Furthermore, we compared the genome-targeting and gene-modulatory effects by WT Kdm5b versus an enzymatic-dead mutant (H499A). First, we introduced either WT or mutant forms of Kdm5b into HEK293 cells because this cell line is generally insensitive to Kdm5b expression and thus allows comparison of WT versus mutant Kdm5b without being affected by cell status changes (such as differentiation and proliferation seen with AML). CUT&RUN results for WT and H499A-mutated Kdm5b revealed comparable binding at target genes (Fig. 6 *D* and *E*), as exemplified by Kdm5b peaks at AML-related genes such as *MN1*, *HOX-A* cluster genes, *SOX4*, and *CCND2/3* (Fig. 6*F* and *SI Appendix*, Fig. S5*A*). Complementary to the genomic binding results, RNA-seq analyses further confirmed that gene-modulatory effects of WT and H499A-mutated Kdm5b are largely comparable in MLL-AF9$^+$ murine AML cells (Dataset S6), with there being a significant overlap between differentially expressed genes (DEGs), either down- or up-regulated, following stable expression of either form of Kdm5b (Fig. 6*G* and *SI Appendix*, Fig. S5*B*). Again, GSEA of RNA-seq datasets confirmed that both WT Kdm5b and its H499A mutant show a positive correlation with the slowed cell cycle progression and increased cell death (Fig. 6*H* and *SI Appendix*, Fig. S5*C*). Equally repressive effects of WT and H499A-mutated Kdm5b on the tested AML oncogenes (Sox4, Ccnd2, and Hmgb3) were also verified by qRT-PCR (Fig. 6*I*).

Taken together, our results demonstrate a striking similarity between WT Kdm5b and its demethylase-dead mutant in terms of AML growth suppression, chromatin binding, cofactor interaction (such as HDAC1), and gene-expression modulation.

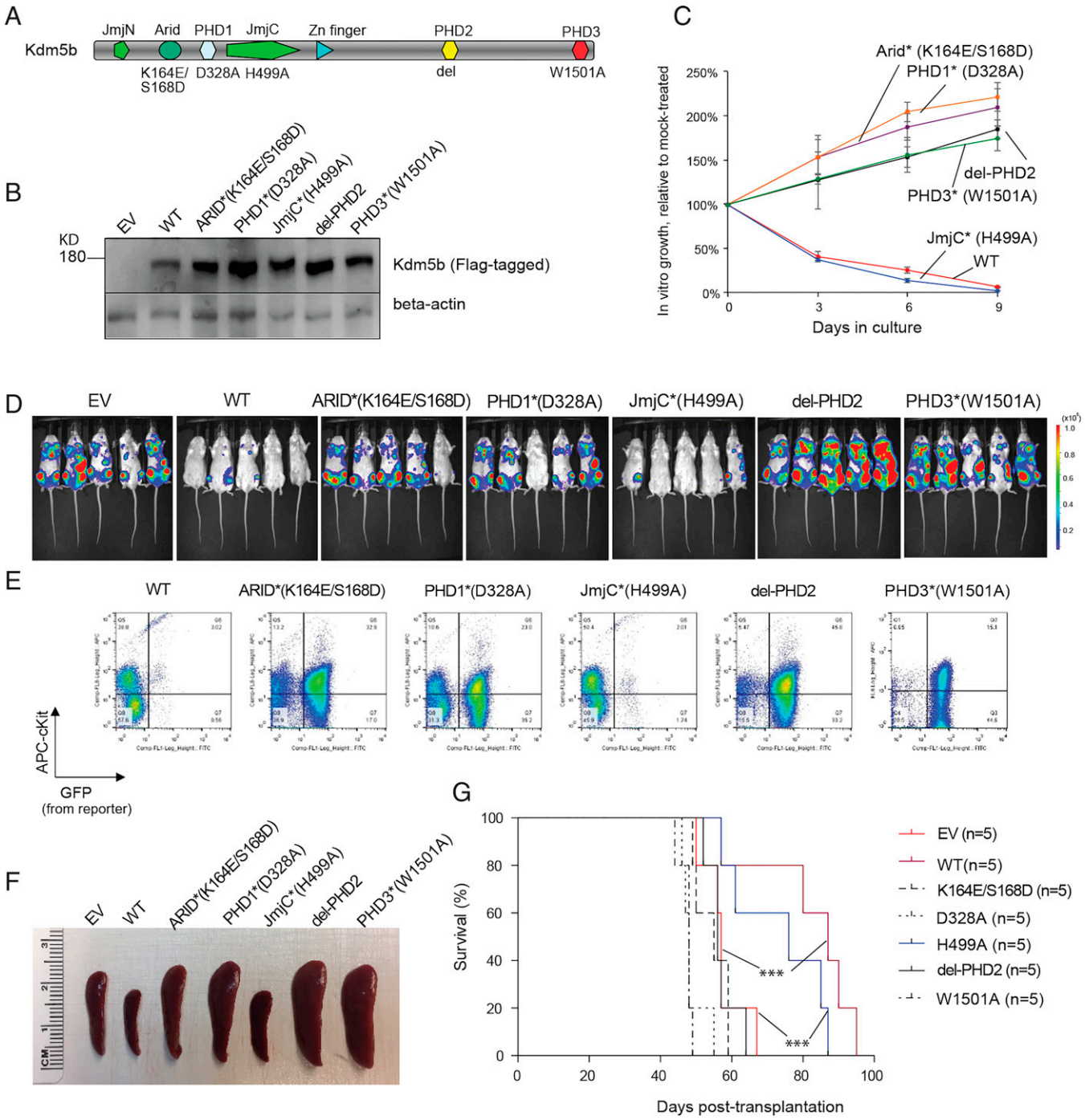

Fig. 5. The chromatin association and/or scaffolding function of Kdm5b is essential for its tumor-suppressive effect in AML, whereas its intrinsic demethylase activity is dispensable. (*A*) Protein architecture of Kdm5b, with its functional domains and used mutations labeled on the *Top* and *Bottom*, respectively. del, deletion. (*B*) Anti-Flag immunoblotting of WT and mutant Flag-tagged Kdm5b after stable expression in cells. (*C*) Proliferation of NUP98-NSD1$^+$ murine AML cells after stable transduction of WT or mutant Kdm5b, relative to EV. The *y*-axis represents relative percentage of cell numbers normalized to EV-expressing controls ($n = 3$ independent experiments; presented as mean ± SD). Star indicates the domain mutation. (*D–G*) Effect of ectopically expressed Kdm5b, either WT or mutant, on AML leukemogenesis. NUP98-NSD1$^+$ murine AML cells carrying a luciferase-IRES-GFP reporter were stably transduced with the indicated Kdm5b and then transplanted intravenously into syngeneic mice. Leukemogenesis was monitored by chemiluminescence imaging of live animals (30 d posttransplantation; *D*), FACS (*E*) of the isolated bone marrow cells (cKit$^+$GFP$^+$ indicates in vivo expansion of GFP-labeled NUP98-NSD1$^+$ AML cells), measurement (*F*) of spleen size (50 d posttransplantation when leukemic mice were close to their terminal stage), and survival curves (*G*) of mice transplanted with the indicated NUP98-NSD1$^+$ AML cells ($n = 5$ per cohort). ***$P < 0.001$. KD, knockdown.

Discussion

AML is an aggressive disease, demanding a better appreciation of the underlying oncogenic mechanisms and improved therapy. Expression of the stem-like gene-expression program in AML is known to be well correlated with poor prognosis (33, 34). How such a transcriptomic feature is maintained in AML has remained unclear. Chromatin modulation is increasingly appreciated as a major molecular determinant for the

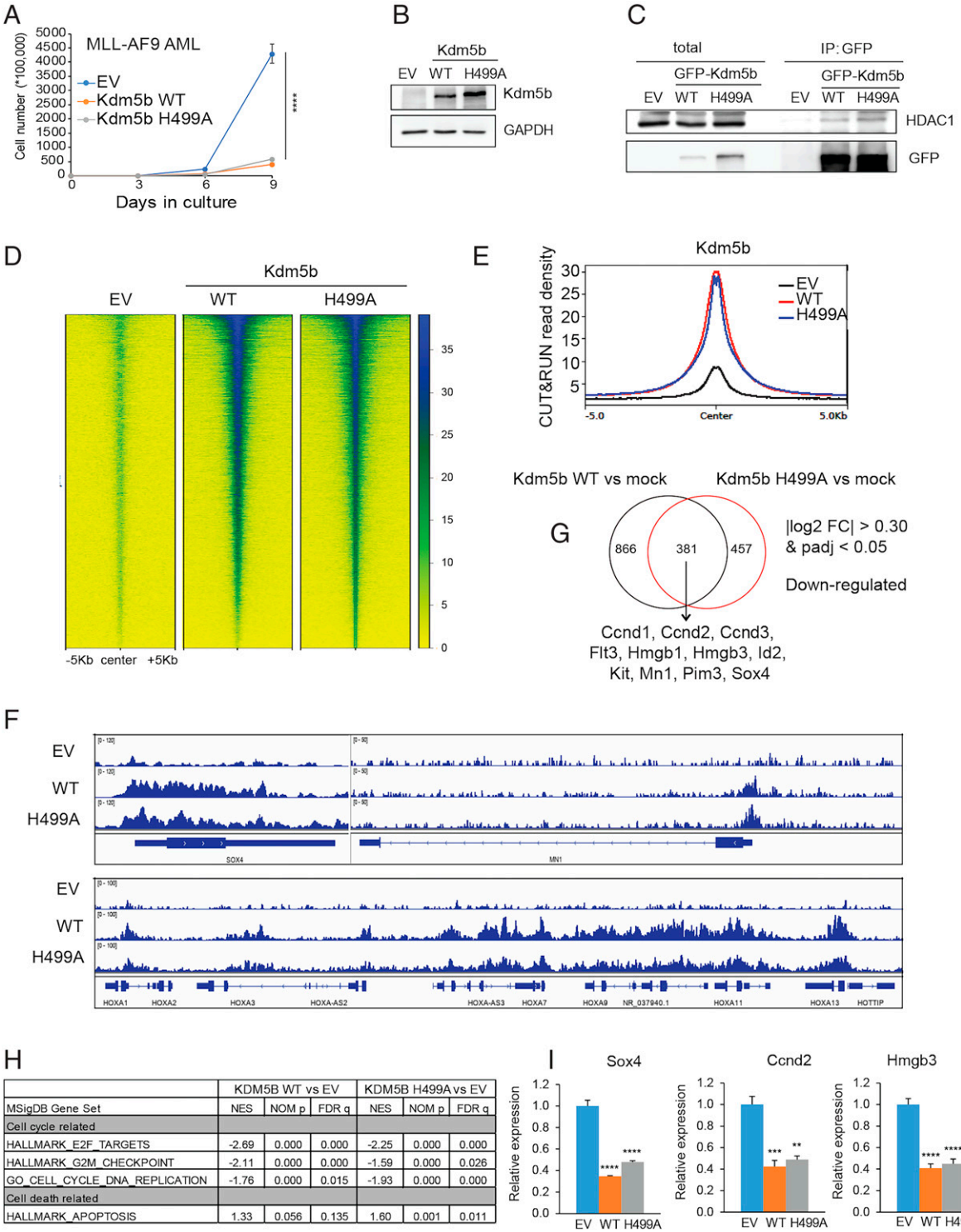

	KDM5B WT vs EV			KDM5B H499A vs EV		
MSigDB Gene Set	NES	NOM p	FDR q	NES	NOM p	FDR q
Cell cycle related						
HALLMARK_E2F_TARGETS	-2.69	0.000	0.000	-2.25	0.000	0.000
HALLMARK_G2M_CHECKPOINT	-2.11	0.000	0.000	-1.59	0.000	0.026
GO_CELL_CYCLE_DNA_REPLICATION	-1.76	0.000	0.015	-1.93	0.000	0.000
Cell death related						
HALLMARK_APOPTOSIS	1.33	0.056	0.135	1.60	0.001	0.011

Fig. 6. Kdm5b suppresses AML-related gene targets in a demethylase-independent manner. (*A*) Proliferation of MLL-AF9$^+$ murine AML cells transduced with EV or Flag-tagged Kdm5b, either WT or H499A-mutated. The *y*-axis represents accumulative cell numbers ($n = 3$ independent experiments; mean ± SD). ****$P < 0.0001$. (*B*) Immunoblotting for exogenously expressed Kdm5b using cells in (*A*). (*C*) CoIP for HDAC1 interaction with GFP-tagged Kdm5b, WT, or H499A-mutated, in HEK293 cells. IP, immunoprecipitation. (*D* and *E*) Heatmap (*D*) and averaged plotting (*E*) of GFP CUT&RUN signals for WT and H499A-mutated Kdm5b (GFP-tagged) at the peak-centered genomic regions (± 5 kb) in the HEK293 stable expression cells. Non–GFP-tagged cells (EV) act as a background control. (*F*) IGV views showing WT and H499A-mutated Kdm5b CUT&RUN signals at the indicated gene in the HEK293 stable expression cells. (*G*) Venn diagram showing the overlap of DEGs, as determined by RNA-seq to be down-regulated in MLL-AF9$^+$ murine AML cells posttransduction of WT (*Left*) or H499A-mutated (*Right*) Flag-Kdm5b, relative to EV ($n = 2$ replicated samples). AML-related oncogenes and the DEG threshold are indicated. (*H*) GSEA reveals that relative to EV, expression of WT (*Left*) or H499A-mutated (*Right*) Kdm5b is negatively correlated to activation of proliferation-related gene sets in MLL-AF9$^+$ AML cells. NOM p, normalized *p*-values. (*I*) qRT-PCR of the indicated AML-related genes in MLL-AF9$^+$ murine AML cells after ectopic expression of WT or H499A-mutated Kdm5b. The qRT-PCR signals are relative to EV-transduced cells after being normalized to GAPDH ($n = 3$ independent experiments; presented as the mean ± SD). **$P < 0.01$; ***$P < 0.001$; ****$P < 0.0001$. FC, fold-change.

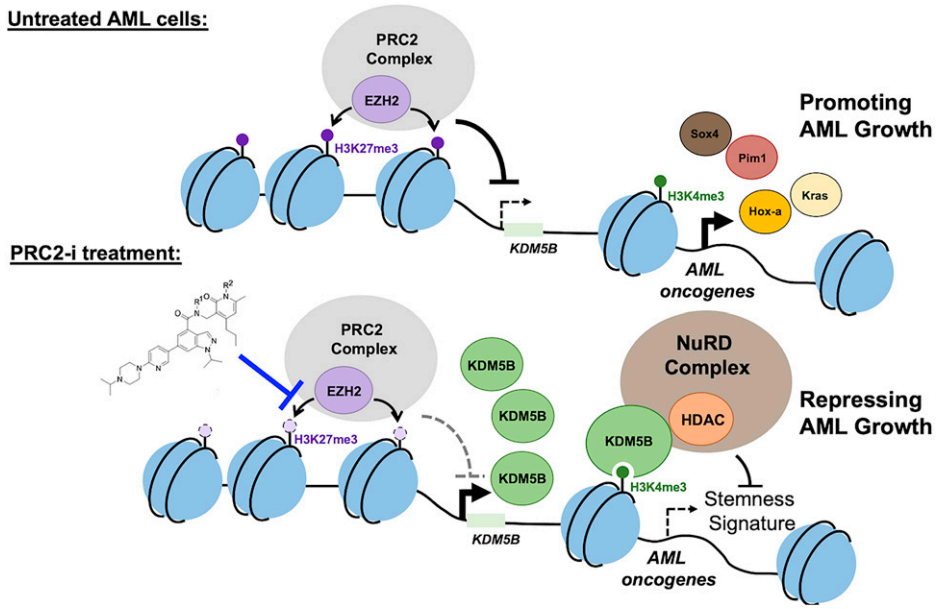

Fig. 7. Scheme showing a role for the PRC2-|KDM5B axis in mediating AML tumorigenesis. Kdm5b is subject to epigenetic repression by PRC2 and H3K27me3, and such a Kdm5b repression is required for sustaining the expression of AML-causing and stemness-related genes, promoting the leukemogenesis initiated by NUP98-NSD1 and MLL-r. Upon treatment with PRC2 inhibitors (PRC2-i) such as UNC1999, the Kdm5b level is elevated. Then, Kdm5b assembles a transcriptional repressive machinery (with HDAC1 and others), leading to the down-regulation of stemness genes and suppression of AML growth. In this scenario, Kdm5b's gene-repressing and anti-AML effects are largely demethylase-independent.

gene-expression patterns and cellular identities, and its dysregulation is frequent in cancer, including AML (9–12, 26, 35). Among various chromatin-modulatory players, PRC2 catalyzes formation of H3K27me3, leading to the silenced chromatin state. Involvement of PRC2 and H3K27me3 in tumorigenesis has been demonstrated with several cancer models, in which the overexpression and/or activating mutation of EZH2 or PRC2 cofactor promotes development of cancers such as AML (13–17, 36, 37), B cell lymphoma (38), melanoma (18), lung cancer (19), and multiple myeloma (39). Here, we report that, in AML subtypes with adverse outcomes (NUP98-NSD1$^+$ or MLL-r$^+$), a PRC2–|*Kdm5b* axis functions to sustain AML tumorigenicity. Integrated profiling showed that Kdm5b and oncogenic AML proteins cobind target genes related to stemness and proliferation, where Kdm5b acts to repress such an oncogenic program. A role for Kdm5b in regulating stemness genes in normal hematopoietic stem/progenitor cells has been reported (40). Consistent with our AML animal data, interrogation of multiple clinical datasets of AML patients supported a strong correlation of the reduced *KDM5B* expression with poorer prognosis. This work not only uncovered a PRC2–|*Kdm5b* pathway underlying AML tumorigenicity and aggressiveness but also provides an explanation for the anti-AML effect of the PRC2 catalytic inhibitors. It is noteworthy to mention that this axis of PRC2–|*Kdm5b*–|oncogenic/stemness transcripts can cooperate with the previously reported pathways enforced by PRC2 and H3K27me3 readers, such as silencing of tumor suppressors (41) and immunity-related genes (42), which collectively establish aggressive features seen in AML (Fig. 7).

While Kdm5b's chromatin association domains (ARID, PHD1, and PHD3 domains) are essential for suppressing AML tumorigenesis, its demethylation activity is unexpectedly dispensable for the anti-AML effects of Kdm5b both in vitro and in vivo. In this regard, a recent investigation pointed to a role for KDM5B in suppressing the expression of endogenous retroelements such as MMVL30 in mouse melanoma models (43), with the immunity-inhibiting effect of KDM5B being mediated by recruitment of the H3K9 methyltransferase SETDB1 and not by its intrinsic demethylase activity. Thus, the target-repressing activities of KDM5B are often demethylase-independent, as seen at endo-retrovirus elements in melanoma (43) and stemness genes in AML. We further show that Kdm5b's genome-targeting and cofactor (HDAC1) interaction are unaffected by an enzymatic-dead mutation (H499A). We thus favor a model in which Kdm5b functions as a scaffold protein to mediate the recruitment and/or assembly of a gene-repressive complex (HDAC-containing SIN3B and NuRD or other gene-repressive complexes) at AML oncogenes, thereby attenuating the leukemogenesis.

KDM5's PHD1 and PHD3 carry histone tail-binding activities (22, 26). It has been suggested that the KDM5 PHD2 may serve as a part of the structural linker in forming a "dumbbell shaped and curved" KDM5B architecture (44), although its exact role merits further investigation. The PHD3-containing fragment of KDM5A (a functionally related KDM5B family protein) was found to be recurrently fused to NUP98 in a subset of AMLs, driving AML development (26, 45). In this scenario, the resultant NUP98-KDM5A(PHD3) oncoproteins (or similar chimeras) bind H3K4me3 (via the H3K4me3-binding PHD3) and can form phase-separated protein condensate (6), leading to maintenance of high expression of a suite of stemness and leukemogenic genes (25–27). Thus, the H3K4me3/2-binding activity harbored within PHD3 is important for both NUP98-KDM5A fusion and normal KDM5B. It is very likely that disruption of one normal KDM5A allele by a NUP98-KDM5A chromosomal translocation contributes to the aggressive features of AML, which requires additional investigation. Interestingly, interrogation of KDM5B and KDM5A using cBioPortal revealed low rates of deletion or somatic mutation among patients of myeloid malignancy and AML (*SI Appendix*, Fig. S6*A*). Mutations of these functionally related genes show a tendency of enrichment at a region encoding the chromatin-binding and structural domains (*SI Appendix*, Fig. S6 *B* and *C*), such as PHD3 and a PLU1 domain suggested to be a structural "tower region" (44).

Deregulation of lysine demethylases is a recurrent theme in cancers (12, 46). KDMs may have both tumor-promoting and -suppressive roles. On the one hand, KDM5 family proteins

can be oncogenic in solid tumors, including breast cancer and melanoma (47–49). As an example, KDM5B can silence tumor immunity-associated pathways (43). On the other hand, tumor-suppressing roles for KDM5 have been demonstrated in solid tumors such as breast cancer (22, 31), consistent with its AML-suppressing function shown in this work. The functions of KDM5 proteins are multifaceted and subject to further investigation.

Materials and Methods

Plasmid construction, tissue culture and cell lines, antibodies and Western blotting, chemicals, phenotypic assays of hematological cells, such as colony-forming units (CFUs), Wright-Giemsa staining and proliferation assays, assays of cell cycle progression and apoptosis, the in vivo leukemogenic studies, RNA sequencing and data analysis, ChIP-seq and data analysis, CUT&RUN and data analysis, analysis of publicly available patient datasets, qRT-PCR, and statistics and reproducibility can be found in *SI Appendix, Materials and Methods*. All animal experiments were performed according to the protocol approved by Institutional Animal Care and Use Committee, University of North Carolina UNC).

Data Availability. All study data are included in the article and/or supporting information. RNA-seq, ChIP-seq, and CUT&RUN datasets related to this work have been deposited in the National Center for Biotechnology Information (NCBI) Gene Expression Omnibus (GEO) under accession number GSE179826.

ACKNOWLEDGMENTS. We thank Drs. Qin Yan and David L. Bentley for providing reagents used in the study and all laboratory members for discussion and technical support. We sincerely thank UNC facilities, including the High-Throughput Sequencing Facility, Bioinformatics Core, Flow Cytometry Core, Tissue Culture Facility, and Animal Studies Core, for their professional assistance of this work. The cores affiliated with the UNC Cancer Center are supported in part by the UNC Lineberger Comprehensive Cancer Center Core Support Grant P30-CA016086. The publicly available The Cancer Genome Atlas (TCGA) dataset used here is in whole or part based upon data generated by the TCGA Research Network: https://www.cancer.gov/tcga. This work was supported by NIH (CA178765, to R.G.R.), the Leukemia and Lymphoma Society Specialized Center of Research Grant (17403-19, to R.G.R.), the Gilead Sciences Research Scholars Program in hematology/oncology (to G.G.W.), When Everyone Survives Leukemia Research Foundation (to G.G.W.), the Ministry of Science and Technology in Taiwan (MOST 107-2320-B-010-024-MY3 and 110-2320-B-A49A-533-MY3, to W.-Y.C.), and the Cancer Progression Research Center, National Yang Ming Chiao Tung University, from the Featured Areas Research Center Program within the framework of the Higher Education Sprout Project by the Ministry of Education in Taiwan (to W.-Y.C.).

1. N. Shiba *et al.*, NUP98-NSD1 gene fusion and its related gene expression signature are strongly associated with a poor prognosis in pediatric acute myeloid leukemia. *Genes Chromosomes Cancer* **52**, 683–693 (2013).
2. I. H. Hollink *et al.*, NUP98/NSD1 characterizes a novel poor prognostic group in acute myeloid leukemia with a distinct HOX gene expression pattern. *Blood* **118**, 3645–3656 (2011).
3. F. Ostronoff *et al.*, NUP98/NSD1 and FLT3/ITD coexpression is more prevalent in younger AML patients and leads to induction failure: A COG and SWOG report. *Blood* **124**, 2400–2407 (2014).
4. B. V. Balgobind, C. M. Zwaan, R. Pieters, M. M. Van den Heuvel-Eibrink, The heterogeneity of pediatric MLL-rearranged acute myeloid leukemia. *Leukemia* **25**, 1239–1248 (2011).
5. R. C. Rao, Y. Dou, Hijacked in cancer: The KMT2 (MLL) family of methyltransferases. *Nat. Rev. Cancer* **15**, 334–346 (2015).
6. J. H. Ahn *et al.*, Phase separation drives aberrant chromatin looping and cancer development. *Nature* **595**, 591–595 (2021).
7. G. G. Wang, L. Cai, M. P. Pasillas, M. P. Kamps, NUP98-NSD1 links H3K36 methylation to Hox-A gene activation and leukaemogenesis. *Nat. Cell Biol.* **9**, 804–812 (2007).
8. A. V. Krivtsov, S. A. Armstrong, MLL translocations, histone modifications and leukaemia stem-cell development. *Nat. Rev. Cancer* **7**, 823–833 (2007).
9. A. H. Shih, O. Abdel-Wahab, J. P. Patel, R. L. Levine, The role of mutations in epigenetic regulators in myeloid malignancies. *Nat. Rev. Cancer* **12**, 599–612 (2012).
10. B. Xu, K. D. Konze, J. Jin, G. G. Wang, Targeting EZH2 and PRC2 dependence as novel anticancer therapy. *Exp. Hematol.* **43**, 698–712 (2015).
11. P. Chi, C. D. Allis, G. G. Wang, Covalent histone modifications–miswritten, misinterpreted and mis-erased in human cancers. *Nat. Rev. Cancer* **10**, 457–469 (2010).
12. S. Zhao, C. D. Allis, G. G. Wang, The language of chromatin modification in human cancers. *Nat. Rev. Cancer* **21**, 413–430 (2021).
13. J. Shi *et al.*, The Polycomb complex PRC2 supports aberrant self-renewal in a mouse model of MLL-AF9;Nras(G12D) acute myeloid leukemia. *Oncogene* **32**, 930–938 (2013).
14. T. Neff *et al.*, Polycomb repressive complex 2 is required for MLL-AF9 leukemia. *Proc. Natl. Acad. Sci. U.S.A.* **109**, 5028–5033 (2012).
15. W. Kim *et al.*, Targeted disruption of the EZH2-EED complex inhibits EZH2-dependent cancer. *Nat. Chem. Biol.* **9**, 643–650 (2013).
16. S. Tanaka *et al.*, Ezh2 augments leukemogenicity by reinforcing differentiation blockage in acute myeloid leukemia. *Blood* **120**, 1107–1117 (2012).
17. B. Xu *et al.*, Selective inhibition of EZH2 and EZH1 enzymatic activity by a small molecule suppresses MLL-rearranged leukemia. *Blood* **125**, 346–357 (2015).
18. G. P. Souroullas *et al.*, An oncogenic Ezh2 mutation induces tumors through global redistribution of histone 3 lysine 27 trimethylation. *Nat. Med.* **22**, 632–640 (2016).
19. H. Zhang *et al.*, Oncogenic deregulation of EZH2 as an opportunity for targeted therapy in lung cancer. *Cancer Discov.* **6**, 1006–1021 (2016).
20. S. H. Wong *et al.*, The H3K4-methyl epigenome regulates leukemia stem cell oncogenic potential. *Cancer Cell* **28**, 198–209 (2015).
21. Y. Zhang *et al.*, The PHD1 finger of KDM5B recognizes unmodified H3K4 during the demethylation of histone H3K4me2/3 by KDM5B. *Protein Cell* **5**, 837–850 (2014).
22. B. J. Klein *et al.*, The histone-H3K4-specific demethylase KDM5B binds to its substrate and product through distinct PHD fingers. *Cell Rep.* **6**, 325–335 (2014).
23. S. Yamamoto *et al.*, JARID1B is a luminal lineage-driving oncogene in breast cancer. *Cancer Cell* **25**, 762–777 (2014).
24. B. L. Kidder, G. Hu, K. Zhao, KDM5B focuses H3K4 methylation near promoters and enhancers during embryonic stem cell self-renewal and differentiation. *Genome Biol.* **15**, R32 (2014).
25. Y. Zhang *et al.*, Mechanistic insights into chromatin targeting by leukemic NUP98-PHF23 fusion. *Nat. Commun.* **11**, 3339 (2020).
26. G. G. Wang *et al.*, Haematopoietic malignancies caused by dysregulation of a chromatin-binding PHD finger. *Nature* **459**, 847–851 (2009).
27. S. M. Gough *et al.*, NUP98-PHF23 is a chromatin-modifying oncoprotein that causes a wide array of leukemias sensitive to inhibition of PHD histone reader function. *Cancer Discov.* **4**, 564–577 (2014).
28. S. Tu *et al.*, The ARID domain of the H3K4 demethylase RBP2 binds to a DNA CCGCCC motif. *Nat. Struct. Mol. Biol.* **15**, 419–421 (2008).
29. D. J. Seward *et al.*, Demethylation of trimethylated histone H3 Lys4 in vivo by JARID1 JmjC proteins. *Nat. Struct. Mol. Biol.* **14**, 240–242 (2007).
30. P. P. Wong *et al.*, Histone demethylase KDM5B collaborates with TFAP2C and Myc to repress the cell cycle inhibitor p21(cip) (CDKN1A). *Mol. Cell. Biol.* **32**, 1633–1644 (2012).
31. Q. Li *et al.*, Binding of the JmjC demethylase JARID1B to LSD1/NuRD suppresses angiogenesis and metastasis in breast cancer cells by repressing chemokine CCL14. *Cancer Res.* **71**, 6899–6908 (2011).
32. G. Nishibuchi *et al.*, Physical and functional interactions between the histone H3K4 demethylase KDM5A and the nucleosome remodeling and deacetylase (NuRD) complex. *J. Biol. Chem.* **289**, 28956–28970 (2014).
33. K. Eppert *et al.*, Stem cell gene expression programs influence clinical outcome in human leukemia. *Nat. Med.* **17**, 1086–1093 (2011).
34. L. I. Shlush *et al.*, Tracing the origins of relapse in acute myeloid leukaemia to stem cells. *Nature* **547**, 104–108 (2017).
35. M. A. Dawson, T. Kouzarides, B. J. Huntly, Targeting epigenetic readers in cancer. *N. Engl. J. Med.* **367**, 647–657 (2012).
36. E. Danis *et al.*, Inactivation of Eed impedes MLL-AF9-mediated leukemogenesis through Cdkn2a-dependent and Cdkn2a-independent mechanisms in a murine model. *Exp. Hematol.* **43**, 930–935.e6 (2015).
37. A. T. Thiel, Z. Feng, D. K. Pant, L. A. Chodosh, X. Hua, The trithorax protein partner menin acts in tandem with EZH2 to suppress C/EBPα and differentiation in MLL-AF9 leukemia. *Haematologica* **98**, 918–927 (2013).
38. W. Béguelin *et al.*, EZH2 is required for germinal center formation and somatic EZH2 mutations promote lymphoid transformation. *Cancer Cell* **23**, 677–692 (2013).
39. Z. Ren *et al.*, PHF19 promotes multiple myeloma tumorigenicity through PRC2 activation and broad H3K27me3 domain formation. *Blood* **134**, 1176–1189 (2019).
40. S. Cellot *et al.*, RNAi screen identifies Jarid1b as a major regulator of mouse HSC activity. *Blood* **122**, 1545–1555 (2013).
41. K. H. Kim, C. W. Roberts, Targeting EZH2 in cancer. *Nat. Med.* **22**, 128–134 (2016).
42. M. L. Burr *et al.*, An evolutionarily conserved function of polycomb silences the MHC Class I antigen presentation pathway and enables immune evasion in cancer. *Cancer Cell* **36**, 385–401 (2019).
43. S. M. Zhang *et al.*, KDM5B promotes immune evasion by recruiting SETDB1 to silence retroelements. *Nature* **598**, 682–687 (2021).
44. J. Dorosz *et al.*, Molecular architecture of the Jumonji C family histone demethylase KDM5B. *Sci. Rep.* **9**, 4019 (2019).
45. J. D. de Rooij *et al.*, NUP98/JARID1A is a novel recurrent abnormality in pediatric acute megakaryoblastic leukemia with a distinct HOX gene expression pattern. *Leukemia* **27**, 2280–2288 (2013).
46. R. J. Klose, E. M. Kallin, Y. Zhang, JmjC-domain-containing proteins and histone demethylation. *Nat. Rev. Genet.* **7**, 715–727 (2006).
47. K. Hinohara *et al.*, KDM5 Histone demethylase activity links cellular transcriptomic heterogeneity to therapeutic resistance. *Cancer Cell* **34**, 939–953 (2018).
48. M. Vinogradova *et al.*, An inhibitor of KDM5 demethylases reduces survival of drug-tolerant cancer cells. *Nat. Chem. Biol.* **12**, 531–538 (2016).
49. A. Roesch *et al.*, Overcoming intrinsic multidrug resistance in melanoma by blocking the mitochondrial respiratory chain of slow-cycling JARID1B(high) cells. *Cancer Cell* **23**, 811–825 (2013).

PNAS
www.pnas.org

Supplementary Information for

A PRC2-KDM5B axis sustains tumorigenicity of acute myeloid leukemia

Zhihong Ren[a,b,1,#], Arum Kim[a,b,1], Yu-Ting Huang[c,2], Wen-Chieh Pi[c,2], Weida Gong[a], Xufen Yu[d], Jun Qi[e], Jian Jin[d], Ling Cai[a,b,f], Robert G. Roeder[g,3], Wei-Yi Chen[c,h,3], Gang Greg Wang[a,b,i,3]

[3]Correspondence authors:
Robert G. Roeder
Contact: roeder@rockefeller.edu

Wei-Yi Chen
Contact: chenwy@nycu.edu.tw

Gang Greg Wang
Contact: greg_wang@med.unc.edu

This PDF file includes:

Supplementary Materials and Methods

Plasmid construction

The cDNA of murine *Kdm5b* (NM_152895.2) was cloned into the MSCV-puro retroviral vector, with Flag or GFP tag added in-frame to its N-terminus. *Kdm5b* mutants were created by site-directed mutagenesis as described before [1, 2]. For knockdown (KD) of murine *Kdm5b* (Sigma, cat# TRCN0000113491; with the hairpin sequence as GCCTACATCATGTGAAAGAAT) or human *EZH2* gene (Sigma, cat# TRCN0000018365; with the hairpin sequence as TATGATGGTTAACGGTGATCA), the pLKO.1-puro based lentiviral shRNA was purchased from Sigma and used according to vendor-recommended manuals.

Tissue culture and cell lines

Murine AML cell lines carrying NUP98-NSD1 (Flag-tagged) or MLL-r were previously described [3-5]. In brief, lineage-negative hematopoietic stem and progenitor cells (HSPCs) isolated from BALB/C mice were stably transduced with the oncogene, followed by transplantation to syngeneic mice. The murine AML cells were derived from bone marrow of leukemic mice and maintained in the OptiMEM base medium supplemented with 15% of FBS, 50uM of beta-mercaptoethanol, 1% of penicillin and streptomycin, and murine stem cell factor (mSCF; added with 10% of supernatant from a mSCF-secreting Chinese hamster ovary cell line). Human cell lines including MV4;11 (American Tissue Culture Collection [ATCC], CRL-9591), MOLM13 (Deutsche Sammlung von Mikroorganismen und Zellkulturen [DSMZ], ACC-554) and HEK293T (ATCC CRL-3216) were maintained using vendor-recommended culture conditions. To establish the stable cell lines, retrovirus or lentivirus was prepared with the packaging system in HEK293T cells, followed by cell infection and drug selection as we described before [1, 2, 6]. Authentication of cell line identities was ensured by the Tissue Culture Facility (TCF) affiliated to UNC Lineberger Comprehensive Cancer Center with the genetic signature profiling analysis. Every 1-2 months, a routine examination of cells for potential mycoplasma contamination was performed using the commercially available detection kits (Lonza).

Antibodies and western blot

The immunoblotting was conducted with the total cell lysate as we reported before [1, 2, 6]. Antibodies used in this study are listed in Dataset S7.

Chemicals

UNC1999 [5, 7, 8] and JQEZ5 [9, 10] were synthesized and used as previously reported.

Phenotypic assays of hematological cells, such as colony-forming unit (CFU), Wright-Giemsa staining and proliferation assay

Assays for CFU using a methylcellulose-based culture system (STEMCELL Technologies, M3434), Wright-Giemsa staining, and counting-based cell proliferation were carried out as we described before [1, 5, 11].

Assays of cell cycle progression and apoptosis

To measure cell cycle progression, cells were collected by centrifugation, washed with ice-cold PBS, and fixed in pre-chilled 80% methanol. Cell staining was then conducted in PBS plus 20 μg/mL of propidium iodide (Sigma), 0.1% of Triton-X100 and 200 μg/mL of RNase A (Roche). DNA contents of cells were measured with a CyAnADP flow cytometer (Beckman-Coulter) and then analyzed by ModFit Software to define the status of cell cycle progression (VeritySoftware). Apoptosis was measured with the Annexin V-FITC Apoptosis Detection Kit (BD, 556570), followed by analysis with the CyAnADP flow cytometer and then analysis with the FlowJo Software (BD).

In vivo leukemogenic studies

All animal experiments were performed according to the protocol approved by Institutional Animal Care and Use Committee (IACUC), University of North Carolina (UNC). Murine AML was established by injection of 0.5 million of the already established murine AML cell lines (stably labeled with a luciferase-IRES-GFP reporter) via tail vein into syngeneic BALB/C mice (Jackson Laboratory) as described [1, 5, 11]. All mice were housed according to the guidelines of UNC

Animal Studies Core. Animal care, monitoring of leukemogenesis such as weekly chemiluminescence imaging of live animals and treatment with compounds were performed using the same protocols described before [1, 5, 11].

RNA sequencing and data analysis

RNA-seq was performed as previously described [2, 6, 12]. In brief, total RNA was extracted by using RNeasy Plus Mini Kit (Qiagen) and RNA libraries prepared by using the NEBNext Ultra II RNA Library Prep Kit (NEB). Multiplexed RNA-seq libraries were subjected to deep sequencing using the Illumina Hi-Seq 2000/2500 platform according to the manufacturer's instructions (UNC-Chapel Hill High-Throughput Sequencing Facility). Analysis of RNA-seq data and Gene Set Enrichment Analysis (GSEA) with the RNA-seq profiles were conducted as before [1, 2, 6]. In brief, the fastq files were aligned to the mm10 mouse genome (GRCm38.p4) using STAR v2.4.2 [13] with the following parameters: --outSAMtype BAM Unsorted --quantMode TranscriptomeSAM. Transcript abundance for each sample was estimated with salmon v0.1.19 [14] to quantify the transcriptome defined by Ensembl annotation. Gene level counts were summed across isoforms and genes with low counts (maximum expression < 10) were filtered for the downstream analyses. We tested genes for differential expression in DESeq2 v1.38.2 [15].

Chromatin immunoprecipitation (ChIP) followed by sequencing (ChIP-Seq) and data analysis

ChIP-seq was performed according to our previously described protocol [1, 2, 6], with antibodies used in this study are listed in Dataset S7. The produced libraries were subjected to deep sequencing with the Illumina High-Seq 2000/2500 platform according to the manufacturer's instructions (available at the UNC-Chapel Hill High-Throughput Sequencing Facility). ChIP-seq data analysis and profile visualization with Integrative Genomics Viewer (IGV; Broad Institute) were conducted as described before [1, 2, 12, 16].

Analysis of publicly available patient datasets.

The publicly available gene-expression datasets used in the study included the TCGA AML cohort (https://portal.gdc.cancer.gov) and NCBI Gene Expression Omnibus (GEO) accession numbers GSE68833 (TCGA), GSE10358 and GSE14468. To correlate patient clinical outcome with the matched transcriptome profiling, we processed the downloaded datasets with Partek Genomics Suite (Version 6.6), followed by assessment of correlation between gene expression and patient survival as before [7] by using the Kaplan-Meier and Cox survival analysis tools of the Suite according to users' manuals.

RT followed by real-time quantitative PCR (RT-qPCR)

Total RNAs were converted to cDNA with the iScript cDNA Synthesis Kit (Bio-Rad, 1708890). Quantitative PCR was performed in triplicate using the iTaq Universal SYBR Green Supermix (Bio-Rad, 1725124). RT-qPCR was conducted with the QuantStudio 6 Flex real-time PCR system (Applied Biosystems) as described before [7, 17]. Primers used for RT-qPCR are listed in Dataset S7.

Cleavage Under Targets & Release Using Nuclease (CUT&RUN)

CUT&RUN was performed according to manufacturer's instruction (EpiCypher CUTANA™ pAG-MNase for ChIC/CUT&RUN, Cat# 15-1116) as we described [2, 18]. Antibodies used in this study are listed in Dataset S7. In brief, 0.5 million of cells were rinsed with the wash buffer (20 mM HEPES, pH 7.5, 150 mM NaCl, 0.5 mM Spermidine, and 1× Complete Protease Inhibitor Cocktail) and incubated with the activated Concanavalin A (ConA) beads (Bangs Laboratories BP531) at room temperature for 10 minutes, followed by addition of antibody (1:50 dilution) and incubation at 4 degree overnight. After permeabilization with digitonin buffer (the above wash buffer plus 0.01% digitonin), samples were subject to the digestion with pAG-MNase, and solubilized chromatin released. Then, DNA purification was performed with the PCR cleanup kit (NEB, Monarch PCR & DNA Cleanup Kit, T1030), and DNA libraries prepared by using the NEB Ultra II DNA Library Prep Kit (NEB #E7103). Sequencing was carried out using the Illumina NextSeq 500 Sequencing System and CUT&RUN data analysis conducted as we described before [1, 18].

Statistics and reproducibility

All data from representative experiments (such as western blotting, flow and imaging) were repeated two to three times independently with similar results. Data shown in bar plot are presented as mean ± SD of three independent experiments unless otherwise noted. Statistical analysis was performed with two-sided Student's t test for comparing two sets of data with assumed normal distribution. We used a two-sided log-rank test for Kaplan-Meier survival curves to determine statistical significance. A *P* value of less than 0.05 was considered significant. Statistical significance levels are denoted as follows: **P* <0.05; ***P* <0.01; ****P* <0.001; *****P* <0.0001. No statistical methods were used to predetermine sample size.

Data availability

RNA-seq, ChIP-seq and CUT&RUN datasets related to this work have been deposited in the NCBI GEO under accession number GSE179826.

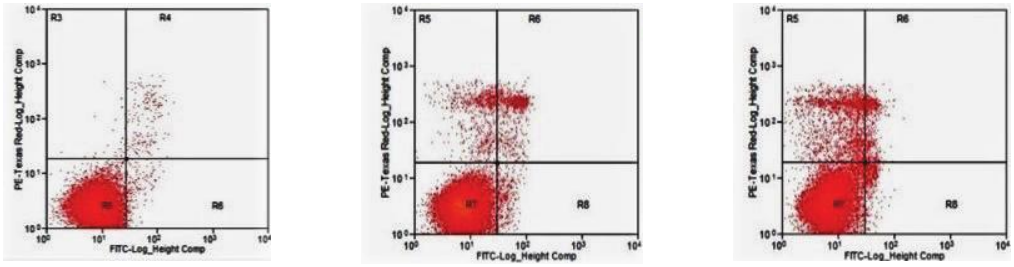

DMSO

UNC1999 1uM
3 days

UNC1999 3uM
3 days

Fig. S1. The representative flow cytometric diagram for assessing apoptotic phenotypes in NUP98-NSD1+ AML cells after treatment with UNC1999.

A

Sample	Replicate #	Total # of reads	# of uniquely mapped reads
DMSO	1	17,547,162	13,729,853
	2	15,474,280	12,134,636
	3	17,412,284	13,621,136
JQEZ5	1	21,220,639	16,814,569
	2	18,507,576	14,744,874
	3	17,437,536	13,800,911
UNC1999	1	19,438,321	15,525,318
	2	17,189,265	13,857,790
	3	14,240,679	11,509,537

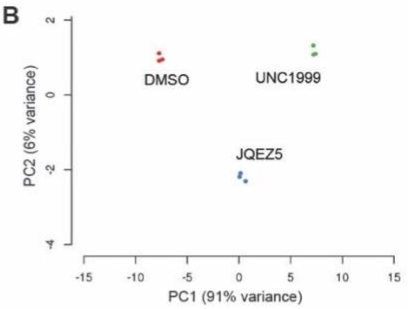

C

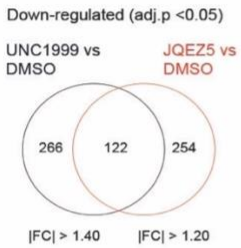

D

	DMSO vs UNC1999			DMSO vs JQ-EZ5		
MSigDB Gene Set	NES	NOM p	FDR q	NES	NOM p	FDR q
Polycomb-related						
PRC2_EED2_UP.V1_DN	1.340	0.018	0.088	1.450	0.000	0.019
PRC2_EZH2_UP.V1_UP	-1.380	0.000	0.039	-1.830	0.000	0.000
Cell cycle related						
HALLMARK_E2F_TARGETS	1.780	0.000	0.002	2.850	0.000	0.000
HALLMARK_G2M_CHECKPOINT	1.710	0.000	0.002	2.480	0.000	0.000
Cell death related						
HALLMARK_APOPTOSIS	-1.520	0.003	0.026	-1.550	0.004	0.010
Hematopoietic stem cell related						
JAATINEN_HEMATOPOIETIC_STEM_CELL_DN	-1.620	0.000	0.093	-2.010	0.000	0.000
Leukemia related						
GO_MYELOID_LEUKOCYTE_DIFFERENTIATION	-1.300	0.045	0.267	-1.620	0.003	0.021

E

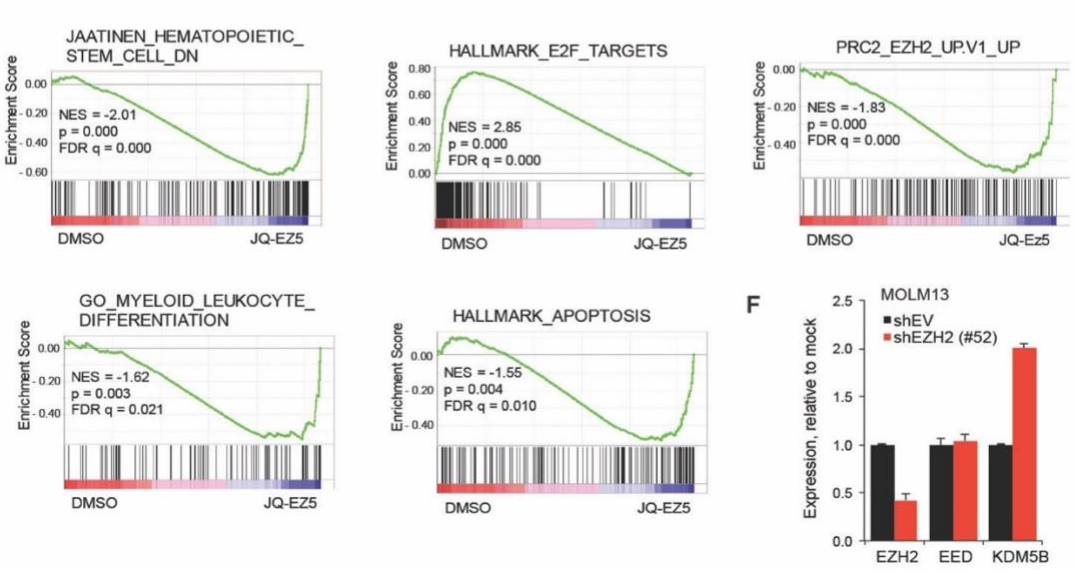

F

Fig. S2. Kdm5b, a tumor suppressor of AML, is a direct target of PRC2 and H3K27me3 in AML. (A-B) Summary of sequencing read counts (A) and Principal Component Analysis (PCA) using RNA-seq data of NUP98-NSD1+ AML cells treated with DMSO, 3 μM of UNC1999 or JQEZ5 for 3 days (n =3 replicated experiments). (C) Venn diagram showing the overlap between differentially expressed genes (DEGs) identified by RNA-seq to be down-regulated after a 3-day treatment with 3 μM of either EZH2 inhibitor, UNC1999 (left) or JQEZ (right), versus DMSO in NUP98-NSD1+ murine AML cells. (D) Summary of Gene Set Enrichment Analysis (GSEA) using the Molecular Signatures Database (MSIgDB), which reveals the indicated gene sets to be correlated with treatment of UNC1999 (left) or JQEZ5 (right), relative to mock. (E) GSEA revealing that JQEZ5 treatment is correlated positively to gene sets repressed by PRC2 or related to leukocyte differentiation or apoptosis in NUP98-NSD1+ murine AML cells. (F) RT-qPCR of EZH2, EED and Kdm5b following EZH2 depletion (shEZH2 #52) in the MOLM-13 human AML cells carrying MLL-r+.

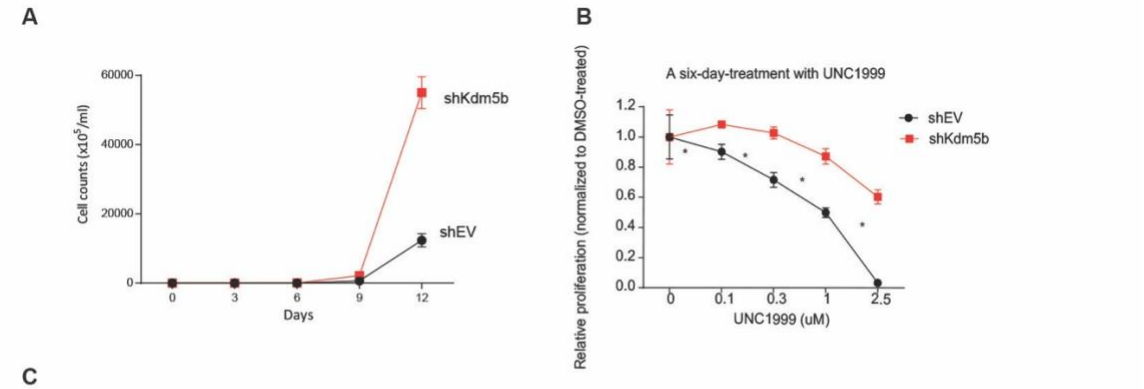

C

	EV vs Kdm5b KD		
MSigDB Gene Set	**NES**	**NOM p**	**FDR q**
Hematopoietic stem cell related			
GO_HEMATOPOIETIC_STEM_CELL_DIFFERENTIATION	1.83	0.000	0.005
RAMALHO_STEMNESS_DN	1.75	0.002	0.011
GO_REGULATION_OF_STEM_CELL_DIFFERENTIATION	1.53	0.010	0.051
Histone methylation related			
MIKKELSEN_ES_ICP_WITH_H3K4ME3	-1.82	0.000	0.008

D

	Kdm5b_exp. vs EV		
MSigDB Gene Set	**NES**	**NOM p**	**FDR q**
Hematopoietic stem cell related			
RAMALHO_STEMNESS_DN	2.27	0.000	0.000
JAATINEN_HEMATOPOIETIC_STEM_CELL_DN	2.13	0.000	0.000
GAL_LEUKEMIC_STEM_CELL_DN	1.55	0.001	0.045
Histone methylation related			
MIKKELSEN_NPC_HCP_WITH_H3K4ME3_AND_H3K27ME3	-1.62	0.013	0.065
MEISSNER_NPC_HCP_WITH_H3K4ME2_AND_H3K27ME3	-1.54	0.010	0.061
MEISSNER_NPC_HCP_WITH_H3K4ME3_AND_H3K27ME3	-1.52	0.017	0.045
Cell cycle related			
HALLMARK_E2F_TARGETS	-2.69	0.000	0.000
HALLMARK_G2M_CHECKPOINT	-2.11	0.000	0.000
GO_CELL_CYCLE_DNA_REPLICATION	-1.76	0.000	0.015
GO_CELL_CYCLE_G2_M_PHASE_TRANSITION	-1.41	0.000	0.052
Cell death related			
HALLMARK_APOPTOSIS	1.33	0.056	0.135

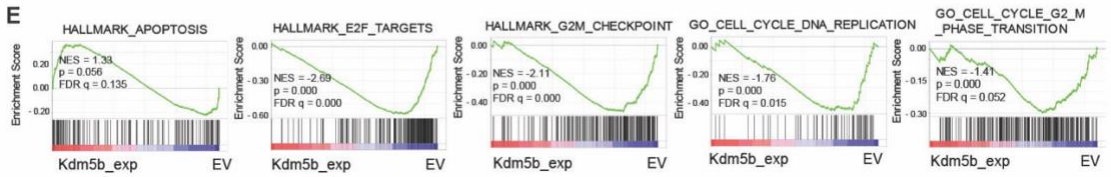

Fig. S3. Depletion of Kdm5b not only renders AML cells unresponsive to PRC2 inhibition but also promotes aggressiveness of AML. (A) Proliferation of NUP98-NSD1-transformed murine AML cells after Kdm5b depletion (shKdm5b), relative to control (shEV; n=3 independent experiments; presented as the mean ± SD). (B) Relative proliferation of the indicated control (shEV) or Kdm5b-depleted (shKdm5b) NUP98-NSD1+ AML cells after treatment with a range of concentrations of UNC1999 for 6 days. Y-axis represents the relative cell numbers normalized to DMSO treatment (n=3 independent experiments; presented as the mean ± SD). *, p<0.05. (C-E) GSEA of RNA-seq profiles revealed that, relative to control (EV), Kdm5b depletion (KD in panel C) is negatively correlated to differentiation-related gene sets while ectopic expression of WT Kdm5b (Kdm5b_exp in panel D) is positively correlated to differentiation- and apoptosis-related gene sets, with the representative GSEA results shown in E.

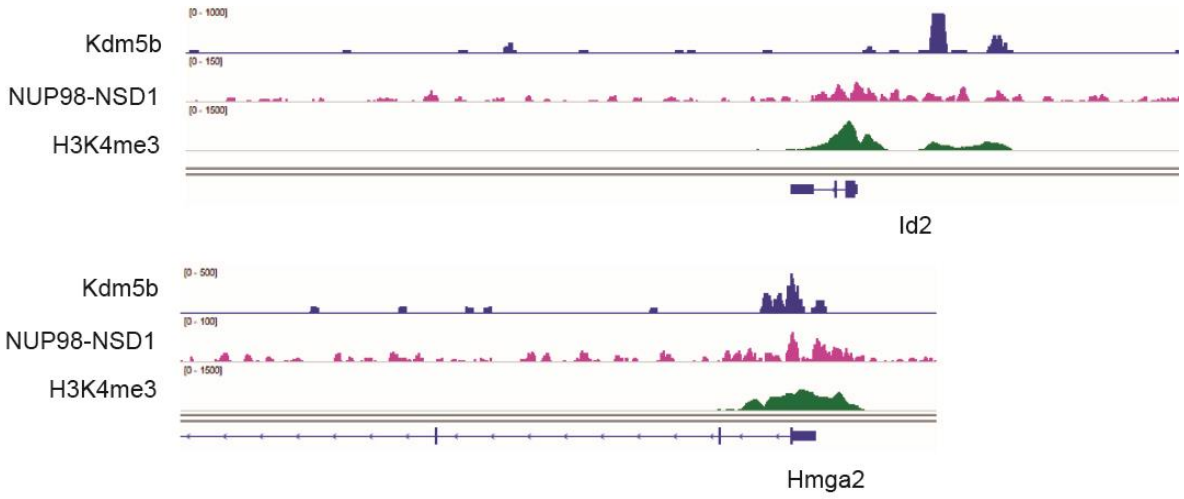

Fig. S4. Kdm5b and NUP98-NSD1 directly bind to stemness and AML-causing genes.
IGV screen shots showing ChIP-seq profiles (after input depth normalization) of Kdm5b, NUP98-NSD1 (Flag-tagged) and H3K4me3 at the indicated cancer-related genes, Id2 and Hmga2, in NUP98-NSD1+ murine AML cells.

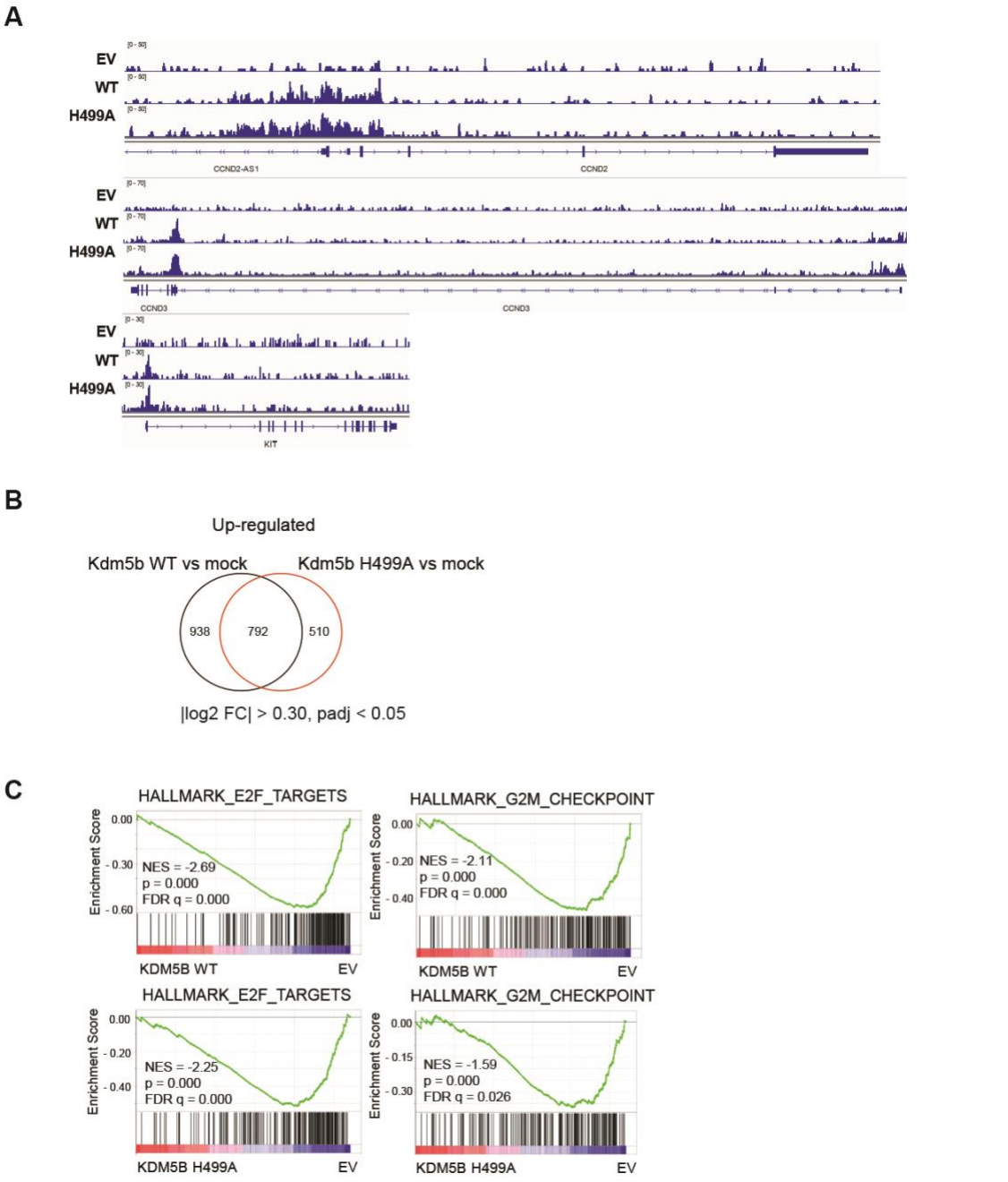

Fig. S5. The demethylase function of Kdm5b is dispensable for its tumor suppressive role in AML. (A) IGV screen shots showing GFP-Kdm5b CUT&RUN profiles at the indicated genes in HEK293 cells with the stable expression of EV (as anti-GFP CUT&RUN control) or GFP-tagged Kdm5b, either WT or H499A-mutated. (B) Venn diagram showing the significant overlap between DEGs found by RNA-seq to be up-regulated post-transduction of WT (left) or H499A-mutated (right) Kdm5b in MLL-AF9+ murine AML cells, relative to EV-transduced mock controls. (C) GSEA of RNA-seq data revealing that, relative to mock controls, ectopic expression of WT (top) or H499A-mutated (bottom) Kdm5b is negatively correlated with cell cycle progression-related gene sets Kdm5b in MLL-AF9+ murine AML cells.

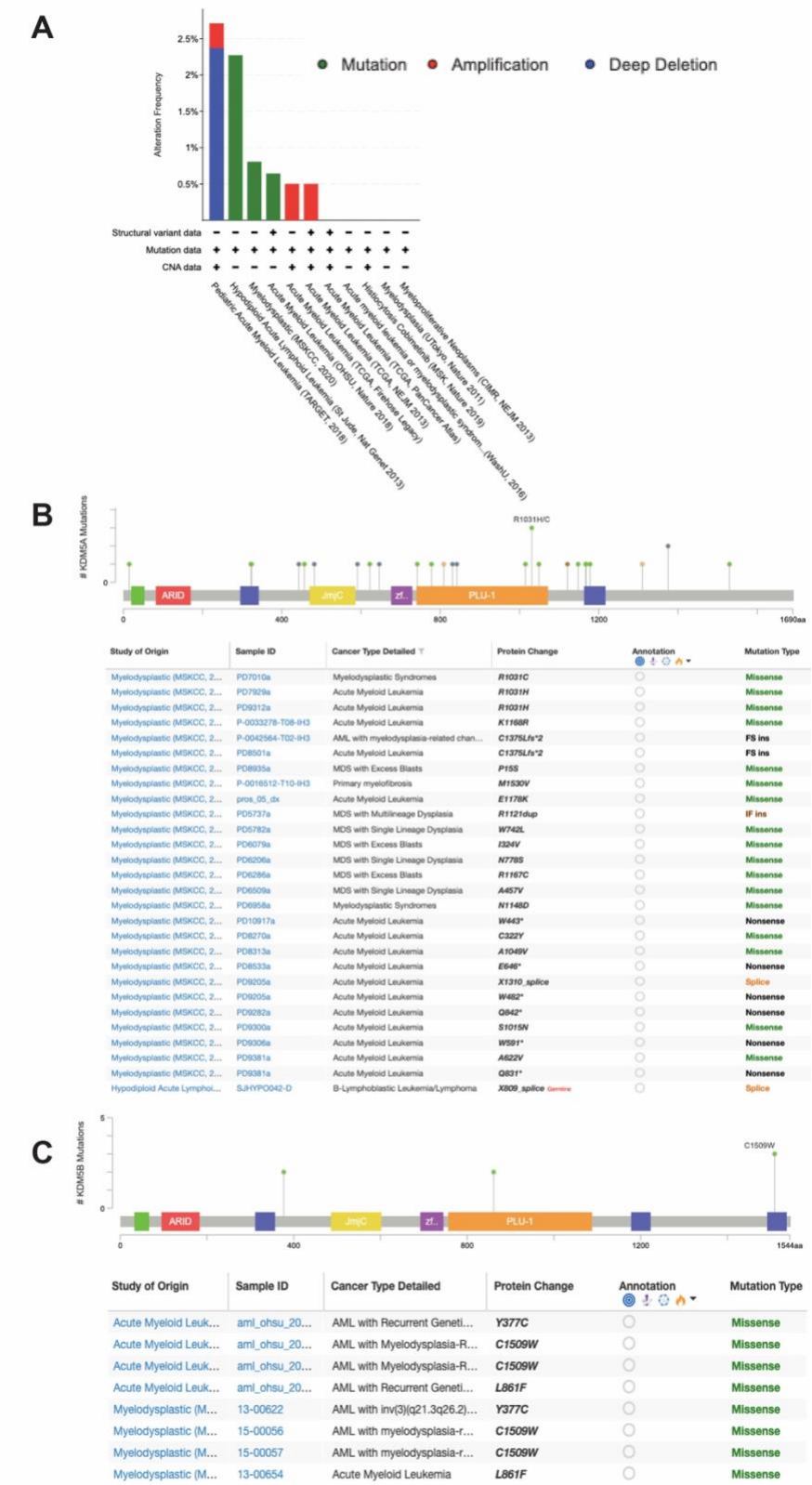

Study of Origin	Sample ID	Cancer Type Detailed	Protein Change	Annotation	Mutation Type
Myelodysplastic (MSKCC, 2...	PD7010a	Myelodysplastic Syndromes	R1031C		Missense
Myelodysplastic (MSKCC, 2...	PD7929a	Acute Myeloid Leukemia	R1031H		Missense
Myelodysplastic (MSKCC, 2...	PD9312a	Acute Myeloid Leukemia	R1031H		Missense
Myelodysplastic (MSKCC, 2...	P-0033278-T08-IH3	Acute Myeloid Leukemia	K1168R		Missense
Myelodysplastic (MSKCC, 2...	P-0042564-T02-IH3	AML with myelodysplasia-related chan...	C1375Lfs*2		FS ins
Myelodysplastic (MSKCC, 2...	PD8501a	Acute Myeloid Leukemia	C1375Lfs*2		FS ins
Myelodysplastic (MSKCC, 2...	PD8935a	MDS with Excess Blasts	P15S		Missense
Myelodysplastic (MSKCC, 2...	P-0016512-T10-IH3	Primary myelofibrosis	M1530V		Missense
Myelodysplastic (MSKCC, 2...	pros_05_dx	Acute Myeloid Leukemia	E1178K		Missense
Myelodysplastic (MSKCC, 2...	PD5737a	MDS with Multilineage Dysplasia	R1121dup		IF ins
Myelodysplastic (MSKCC, 2...	PD5782a	MDS with Single Lineage Dysplasia	W742L		Missense
Myelodysplastic (MSKCC, 2...	PD6079a	MDS with Excess Blasts	I324V		Missense
Myelodysplastic (MSKCC, 2...	PD6206a	MDS with Single Lineage Dysplasia	N778S		Missense
Myelodysplastic (MSKCC, 2...	PD6286a	MDS with Excess Blasts	R1167C		Missense
Myelodysplastic (MSKCC, 2...	PD6509a	MDS with Single Lineage Dysplasia	A457V		Missense
Myelodysplastic (MSKCC, 2...	PD6958a	Myelodysplastic Syndromes	N1148D		Missense
Myelodysplastic (MSKCC, 2...	PD10917a	Acute Myeloid Leukemia	W443*		Nonsense
Myelodysplastic (MSKCC, 2...	PD8270a	Acute Myeloid Leukemia	C322Y		Missense
Myelodysplastic (MSKCC, 2...	PD8313a	Acute Myeloid Leukemia	A1049V		Missense
Myelodysplastic (MSKCC, 2...	PD8533a	Acute Myeloid Leukemia	E646*		Nonsense
Myelodysplastic (MSKCC, 2...	PD9205a	Acute Myeloid Leukemia	X1310_splice		Splice
Myelodysplastic (MSKCC, 2...	PD9205a	Acute Myeloid Leukemia	W482*		Nonsense
Myelodysplastic (MSKCC, 2...	PD9282a	Acute Myeloid Leukemia	Q842*		Nonsense
Myelodysplastic (MSKCC, 2...	PD9300a	Acute Myeloid Leukemia	S1015N		Missense
Myelodysplastic (MSKCC, 2...	PD9306a	Acute Myeloid Leukemia	W591*		Nonsense
Myelodysplastic (MSKCC, 2...	PD9381a	Acute Myeloid Leukemia	A622V		Missense
Myelodysplastic (MSKCC, 2...	PD9381a	Acute Myeloid Leukemia	Q831*		Nonsense
Hypodiploid Acute Lymphoi...	SJHYPO042-D	B-Lymphoblastic Leukemia/Lymphoma	X809_splice Germline		Splice

Study of Origin	Sample ID	Cancer Type Detailed	Protein Change	Annotation	Mutation Type
Acute Myeloid Leuk...	aml_ohsu_20...	AML with Recurrent Geneti...	Y377C		Missense
Acute Myeloid Leuk...	aml_ohsu_20...	AML with Myelodysplasia-R...	C1509W		Missense
Acute Myeloid Leuk...	aml_ohsu_20...	AML with Myelodysplasia-R...	C1509W		Missense
Acute Myeloid Leuk...	aml_ohsu_20...	AML with Recurrent Geneti...	L861F		Missense
Myelodysplastic (M...	13-00622	AML with inv(3)(q21.3q26.2)...	Y377C		Missense
Myelodysplastic (M...	15-00056	AML with myelodysplasia-r...	C1509W		Missense
Myelodysplastic (M...	15-00057	AML with myelodysplasia-r...	C1509W		Missense
Myelodysplastic (M...	13-00654	Acute Myeloid Leukemia	L861F		Missense

Fig. S6. Mutational analyses of KDM5A and KDM5B in samples of AML and myeloid malignancy patients, based on cbioportal. (A) Overall rates of the indicated mutation of KDM5A/B in various myeloid malignancy cohorts. (B-C) Distribution of somatic mutation of KDM5B (B) and KDM5A (C) in the indicated AML or myeloid neoplasm patients.

Table S1. A list of 31 genes showing a common upregulation pattern among NUP98-NSD1- and MLL-AF9-transformed murine AML cells post-treatment of UNC1999, relative to DMSO, and in MLL-AF9+ AML cells post-depletion of Eed versus mock. The transcriptomic data of MLL-AF9+ murine AML cells were from our previously published paper: Supplemental Table S2 in [5]).

Agap1
Arhgap29
B93004
Cdc42bpa
Cdc42bpb
Cdkn2a
Dip2c
Dock7
Exoc6b
F14Rik
Fam46c
Frmd6
Galnt10
Gja1
Glcci1
Kdm5b
Lamc1
Lpl
Nqo1
Plxna1
Rxra
Serpine2
Slc6a8
Slc7a8
Spire1
Tgfbr3
Timp2
Tspan17
Vsig10
Zmat3
Zswim6

Table S2. List of differentially expressed genes (DEGs) showing significant up-regulation post- KD of Kdm5b, relative to mock, in NUP98-NSD1+ murine AML and showing significant down-regulation post-overexpression (OE) of Kdm5b, relative to mock, in MLL-AF9+ murine AML cells. DEGs are defined with a cutoff of adj p value of less than 0.05 and log2(fold-change) of over 0.20 for the genes with baseMean no less than 10. FC, fold change; q, adjusted p value. Red highlighted are genes related to AML stemness and/or aggressive growth.

Snhg17 Bnip3l Itgb7 Strbp Cenpn Rbm3 Gbp7 Tmem218 Sox4 Ttc39c Nol4l Tmsb10 Il1r1 Ankrd37 Gbe1 Dag1 Hmgb3 Lztfl1 Cd33 Tusc3 Mir17hg Sfr1 Arvcf Hnrnph1 Mdm1 Cytip Gm6166 Aldh18a1 Stxbp5 Tuba8 Fancl Rpl36a-ps2 Phf10 Nfix Vegfa 4930427A07Rik Slc7a5 Sh2d5 Ccnd1 Tnk2 Vamp8 Ube2g1 Tmem119 Prss57 Cux1 P4ha1 Anxa2 Pde4d Pold3 Mxd1 Snx30 Vezf1 Rell1 Tgfbr3l Lrrc42 Yars Cnn3 Fabp5 Pfkp Morf4l1 Id2 Fyttd1 C1galt1 Bace1 Pan2 Maff Pdk3 Tgtp2 Antxr2 Palm Gm5537 Pdcd10 Mob3a Mid1 Etv4 Kras Pcgf5 Khnyn Nsd1 Stk26 Btnl9 Rfx2 H2-T23 Fkbp5 Elk3 Ccne2 Kif22 Atp10a Txnip Tpi1 Ero1l Slc2a3 Gm10123 Clic4 Adgrg1 Jarid2 Myo1c Zcchc11 Ifi47 Spns3 Ggta1 Tax1bp1 Ccr1 Mgat5 Tsc22d3 Depdc1a H2-T24 Atf6 Fam160a2 D5Ertd605e Ubald2 Rgcc Oas2 Il12rb2 Muc13 Klhl23 Asap2 Pim1 Arl4a Hnrnph3 Fam63b Rora Acadm Nelfcd Lsm14b Samd9l Cd24a Bcr Uba7 Ift57 Snrpe Tagln2 Add3 Klf10 Mier3 Ptpn22 Ccnd2 Ssbp2 Hmgn5 Mndal Cebpe Flnb Cyb561a3 Otud7b F13a1 Mgat4b Thbs1 Fam133b Eno1 Aldoa Zfp395 Gm13456 Itih5 Pmaip1 Gm4617 Brd3 Tns1 Ramp1 P2ry14 Irf1 App Atp2b4 Cox20 Endod1 A430106G13Rik Trappc9 H1f0 Zc3hav1l Eif4ebp1 Ccnd3 Eno1b Stmn1 Mrpl23 Ptch1 Fam162a Kifap3 Ak4 Casp3 Gpnmb Lgals3 Cmpk2 Higd1a Smad7 Myb H3f3b Nipsnap1 Vps16 1700025G04Rik Treml2 Ksr1 Mxi1 Atf4 Fchsd2 Taf15 Dyrk3 Fcho1 Gadd45a Uimc1 Nos2 Ccnb2 Arhgap18 Vamp3 Lgals9 Pml Vbp1 Mcpt8 Bcl11a S100a8 Plgrkt Pgk1 Cds1 Cxcr2 Glipr2 Sell B4galt4 Prkca Gfod1 Rabgap1l Pdp1 Selp Lsm8 Cntnap1 Sema4b Hmga2 Slc1a4 H2afx Mgat4a Gng12 Nampt Fut7 Icam2 Gm11223 Tia1 Il18rap Elane Sp3 Ppp2r3c Hk1 Pan3 Cdc16 Mphosph6 Nsmaf Cenpk Plppr3 H2-Q7 Cd37 2510002D24Rik

Table S3. List of direct targets co-bound by Kdm5b and NUP98-NSD1, as well as showing significant up-regulation post-KD of Kdm5b, relative to mock, in murine AML cells. DEGs are defined with a cutoff of adj p value of less than 0.05 and log2(fold-change) of over 0.20 for the genes with baseMean no less than 10. FC, fold change; q, adjusted p value. **Red highlighted are genes related to AML stemness and/or aggressive growth.**

Katnbl1 Arhgap29 Nol4l Il10rb Nt5dc1 Fam117b Gnaq Zfp703 Gbe1 Stxbp5 Klf7 Runx2 Tuba8 Six1 Vegfa Ccnl2 Cux1 Vps39 Rabgap1 Rab22a Abtb1 Nphp3 Epm2a Stx6 Akip1 Esyt1 Hnrnpdl Arl8a Dennd3 Pdcd10 Slc32a1 Sh2b3 Znrf1 Plod1 Galnt11 Zc3h6 Ccne2 Stk25 Clic4 Myo1c Samd8 Atg10 Kif1b Fam69a Mtmr2 Tax1bp1 Crtc2 Fam160a2 Mfap3l Cyth1 Lsm14b Kdsr Lgalsl Inpp4a Ulk1 Add3 Map3k5 Fosl2 Gch1 Icosl Inip Ptbp2 Mthfd2l Irf1 Ankrd44 Cox20 Endod1 H1f0 Zc3hav1l Ccnd3 Btbd1 Raph1 Mrpl23 Thra Klhl17 Ddhd2 Med21 Ckap5 Tsc22d1 Kdelr1 Cep120 Kctd20 Snapin Uimc1 Mob1a Ifngr1 Hbp1 Naaa Dmxl2 Prkca Pdp1 Fbxl20 Me2 Sema4b Slc9a8 Mgat4a Gng12 Dtx3 Tia1 Leng8 Ifnar2 Cdkn2c Malt1 Laptm4a Nsmaf 8-Sep Hmg20b Fam117a Qsox2 Pink1 Ypel5 Zfand4 Tbcel Arhgap31 Slc7a5 Tex14 Ccnd1 Vamp8 Pcnx Mctp1 Btg1 Pygl Rnf38 Pold3 Vamp1 Gpt2 Adipor1 Fyn Tfdp2 Ncstn Asah1 Id2 Rsrc1 Sqstm1 Antxr2 Rab18 Fam168a Rcor3 Nr3c1 Hoxa7 Prdm4 Mob3a Kras Nsd1 Uba3 Tex2 Ero1l Rnf11 Paip2b Mgea5 Camkk2 Zswim6 Birc5 Mad2l1 Dleu2 Snrpe Pskh1 Prkch 6820431F20Rik Tmem65 Klf10 Rnf220 Irak1 Plxdc1 Atg16l1 Eno1 Csgalnact2 Dcaf6 Rcbtb2 G2e3 Ccdc69 Irs2 Ano10 Ankrd11 Pank2 Higd1a Smad7 Atf4 Rab5b Phf21a Hspa4l Lockd Fbxo25 Cdc42ep4 Auh 2-Mar Inpp5f Oxr1 Smc4 Emb Tmem181a Mnd1 Rnf19b Pan3 Foxo1 Ccsap Arrdc4 Cyb5r3 Sox4 Nfkbia Ankrd37 Sfr1 Mdm1 Cacna1b Phf10 Cebpg Rb1 Cdk1 Ube2g1 Trim3 Jak2 P4ha1 Rbpj Arsg Dcp1b Vezf1 Phactr4 Pde6d Kctd2 Nrbp1 Mettl23 Rfx2 Fbxl2 E2f6 Ifitm3 Dhrs3 Ptpn12 Msh5 Pias3 Slc44a1 Igf1r Mbtps1 Zfp523 Dcaf12 Hist1h1c Gpcpd1 Clk1 Fndc3b Clcn3 1810026B05Rik Ube2r2 Mapkapk3 Arl4a Spata6 Foxp1 Bcr Casp8 Cmtm3 Ttc17 Wdtc1 Tmbim6 Cebpe B4galt1 Trp53inp1 Klf2 Xpr1 Rsrp1 Otud7b Mgat4b Fam133b Tom1 Plcg1 Lrch1 Rcan3 Klhl5 Crk Hilpda Prkaca Ptch1 Rps23 Cwc15 Fchsd2 Atxn1l Papd4 Dgkg Tm7sf2 Osgin2 Gadd45a Vamp3 Btf3l4 Zfp810 Sft2d2 Cd164 Cds1 Gfod1 Adss Slc1a4 H2afx Nampt Gm16104 Yipf4 Fam45a Rab12 Unc13a E130307A14Rik Tmem229b Arvcf Hnrnph1 Parp8 Smim14 Adcy7 Sh2d5 Scarb2 Dync1li2 Iqsec2 Col5a3 Aplp2 Spag5 Calm2 Zc3h7a Fbxl5 Tm7sf3 Maff Acer3 Phf1 Mob2 Slc38a2 P2rx4 Ldlrad3 H2-T23 Fkbp5 Mbd6 Klf11 Tbc1d2b Pip5k1c Klf13 Jarid2 Zfr2 Furin Hp1bp3 Eef2k Pyroxd2 Pogk Kif23 Pim1 Sec22c Hnrnph3 Mtpn Egln1 Iffo1 Nt5c2 Epha7 Mier3 Tmx4 Cirbp Parp6 Ssbp2 Llgl1 Nfe2l1 Pten Orai1 Asb3 Rac1 Pmaip1 Maml1 Anln St6galnac6 Stmn1 Ddit4 Rufy2 Ksr1 Mxi1 Taf15 Dram1 Lrrfip2 Ccnb2 Atad1 Bcl11a Ube2z Rara Tagap1 Fam103a1 Sike1 Lsm8 Rbl1 Ebag9 Cebpa Inpp1 Cnot6l Ern1 Sp3 Mib2 Bmf

Supplementary References

1. Li, J., et al., *ZMYND11-MBTD1 induces leukemogenesis through hijacking NuA4/TIP60 acetyltransferase complex and a PWWP-mediated chromatin association mechanism.* Nat Commun, 2021. **12**(1): p. 1045.
2. Fan, H., et al., *BAHCC1 binds H3K27me3 via a conserved BAH module to mediate gene silencing and oncogenesis.* Nat Genet, 2020. **52**(12): p. 1384-1396.
3. Wang, G.G., et al., *NUP98-NSD1 links H3K36 methylation to Hox-A gene activation and leukaemogenesis.* Nat Cell Biol, 2007. **9**(7): p. 804-12.
4. Wang, G.G., et al., *Haematopoietic malignancies caused by dysregulation of a chromatin-binding PHD finger.* Nature, 2009. **459**(7248): p. 847-51.
5. Xu, B., et al., *Selective inhibition of EZH2 and EZH1 enzymatic activity by a small molecule suppresses MLL-rearranged leukemia.* Blood, 2015. **125**(2): p. 346-57.
6. Cai, L., et al., *ZFX Mediates Non-canonical Oncogenic Functions of the Androgen Receptor Splice Variant 7 in Castrate-Resistant Prostate Cancer.* Mol Cell, 2018. **72**(2): p. 341-354 e6.
7. Ren, Z., et al., *PHF19 promotes multiple myeloma tumorigenicity through PRC2 activation and broad H3K27me3 domain formation.* Blood, 2019. **134**(14): p. 1176-1189.
8. Konze, K.D., et al., *An orally bioavailable chemical probe of the Lysine Methyltransferases EZH2 and EZH1.* ACS chemical biology, 2013. **8**(6): p. 1324-34.
9. Souroullas, G.P., et al., *An oncogenic Ezh2 mutation induces tumors through global redistribution of histone 3 lysine 27 trimethylation.* Nat Med, 2016. **22**(6): p. 632-40.
10. Zhang, H., et al., *Oncogenic Deregulation of EZH2 as an Opportunity for Targeted Therapy in Lung Cancer.* Cancer Discov, 2016. **6**(9): p. 1006-21.
11. Lu, R., et al., *Epigenetic Perturbations by Arg882-Mutated DNMT3A Potentiate Aberrant Stem Cell Gene-Expression Program and Acute Leukemia Development.* Cancer Cell, 2016. **30**(1): p. 92-107.
12. Yu, X., et al., *A selective WDR5 degrader inhibits acute myeloid leukemia in patient-derived mouse models.* Sci Transl Med, 2021. **13**(613): p. eabj1578.
13. Dobin, A., et al., *STAR: ultrafast universal RNA-seq aligner.* Bioinformatics, 2013. **29**: p. 15-21.
14. Patro, R., et al., *Salmon provides fast and bias-aware quantification of transcript expression.* Nat Methods, 2017. **14**: p. 417-419.
15. Love, M.I., W. Huber, and S. Anders, *Moderated estimation of fold change and dispersion for RNA-seq data with DESeq2.* Genome Biol, 2014. **15**: p. 550.
16. Ahn, J.H., et al., *Phase separation drives aberrant chromatin looping and cancer development.* Nature, 2021. **595**(7868): p. 591-595.
17. Xu, C., et al., *Cistrome analysis of YY1 uncovers a regulatory axis of YY1:BRD2/4-PFKP during tumorigenesis of advanced prostate cancer.* Nucleic Acids Res, 2021. **49**(9): p. 4971-4988.
18. Fan, H., et al., *A conserved BAH module within mammalian BAHD1 connects H3K27me3 to Polycomb gene silencing.* Nucleic Acids Res, 2021. **49**(8): p. 4441-4455.